Miner Deposita (2015) 50:547–569
DOI 10.1007/s00126-014-0558-8

ARTICLE

Stable isotope systematics and fluid inclusion studies in the Cu–Au Visconde deposit, Carajás Mineral Province, Brazil: implications for fluid source generation

Antonia Railine da Costa Silva · Raimundo Netuno Nobre Villas · Jean-Michel Lafon · Gustavo Souza Craveiro · Valderez Pinto Ferreira

Received: 24 October 2013 / Accepted: 22 September 2014 / Published online: 7 October 2014
© Springer-Verlag Berlin Heidelberg 2014

Abstract The Cu–Au Visconde deposit is located in the Carajás Mineral Province (CMP), northern Brazil, near the contact between the ca. 2.76 Ga metavolcano-sedimentary rocks of the Itacaiunas Supergroup rocks and the ~3.0 Ga granitic-gneissic basement. It is hosted by mylonitized Archean rocks, mainly metadacites, the Serra Dourada granite, and gabbros/diorites, which have been successively altered by sodic, sodic-calcic-magnesian, potassic, and calcic-magnesian hydrothermal processes, producing diverse mineralogical associations (albite-scapolite; albite-actinolite-scapolite-epidote; K-feldspar-biotite; chlorite-actinolite-epidote-calcite, etc.). Chalcopyrite is the dominant ore mineral and occurs principally in breccias and veins/veinlets. The aqueous fluids responsible for the alteration/mineralization were initially hot (>460 °C) and very saline (up to 58 wt.% equivalent (equiv.) NaCl), but as the system evolved, they experienced successive dilution processes. Mineral oxygen and hydrogen isotope data show that ^{18}O-rich ($\delta^{18}O_{H_2O} = +4.2$ to +9.4‰) fluids prevailed in the earlier alteration (including magnetitites) and reached temperatures as high as 410–355 °C. Metamorphic/formation waters, most likely derived from the Carajás Basin rocks, appear to have contributed a major component to the fluid composition, although some magmatic input cannot be discounted. In turn, the later alterations and the mineralization involved cooler (<230 °C), ^{18}O-depleted ($\delta^{18}O_{H_2O} = -1.3$ to +3.7‰) and less saline (7–30 wt.% equiv. NaCl) fluids, indicating the influx of meteoric water. Fluid dilution and cooling might have caused abundant precipitation of sulfides, especially as breccia cement. Ore $\delta^{34}S$ values (+0.5 to +3.4‰) suggest a magmatic source for sulfur (from sulfide dissolution in pre-existing igneous rocks). The chalcopyrite Pb–Pb ages (2.73±0.15 and 2.74±0.10 Ga) indicate that the Visconde mineralization is Neoarchean, rather than Paleoproterozoic as previously considered. If so, the hydrothermal processes were synchronous with the 2.75–2.73 Ga transpressive event recorded in the CMP, which is considered the most likely phenomenon that triggered the migration of highly saline fluids trapped in the Carajás Basin rocks.

Keywords Carajás Mineral Province · Cu–Au mineralization · H, O, S isotopes · Fluid inclusions

Editorial handling: D. Craw and G. Beaudoin

A. R. da Costa Silva (✉)
CPRM, Geological Survey of Brazil, Av. André Araújo, 2160, 69060-000 Manaus, AM, Brazil
e-mail: railinegeo@gmail.com

A. R. da Costa Silva · R. N. N. Villas · J.-M. Lafon · G. S. Craveiro
Graduate Program in Geology and Geochemistry, Geosciences Institute, Federal University of Pará-UFPA, Rua Augusto Corrêa, 01, Guamá, P.O. Box 1611, 66075-110 Belém, PA, Brazil

R. N. N. Villas
e-mail: netuno@ufpa.br

J.-M. Lafon
e-mail: lafonjm@ufpa.br

G. S. Craveiro
e-mail: craveiro@ufpa.br

J.-M. Lafon
Laboratory of Isotope Geology (PARÁ-ISO), Geosciences Institute, Federal University of Pará-UFPA, Belém, PA, Brazil

V. P. Ferreira
NEG-LABISE, Deptartment of Geology, Federal University of Pernambuco, P.O. Box 7852, Cidade, Universitária, 50670-000 Recife, PE, Brazil
e-mail: valderez@ufpe.br

Introduction

In the Carajás Mineral Province (CMP), located in the southeastern margin of the Amazon Craton, lies a number of

Precambrian Cu–Au deposits having different metal associations and ages. Noteworthy are the world class (>200 Mt) Igarapé Bahia, Salobo, Sossego (Sequeirinho ore body), and Cristalino deposits, all with substantial magnetite content, which are Archean in age. They have been classified as iron oxide–copper–gold (IOCG) deposits (Tallarico et al. 2005; Monteiro et al. 2008; Grainger et al. 2008; Xavier et al. 2010; Groves et al. 2010; Moreto et al. 2013), although this interpretation is contentious for the Igarapé Bahia deposit (Villas and Santos 2001; Dreher et al. 2008). Smaller IOCG deposits also occur such as the Neoarchean Bacaba, Bacuri and Castanha (Augusto et al. 2008; Pestilho and Monteiro 2008; Moreto et al. 2013), and the Paleoproteozoic Alvo 118 and Sossego orebodies (Tallarico 2003; Torresi et al. 2012; Moreto et al. 2013), in addition to the minor polimetallic (Cu–Au±W–Bi–Sn) Águas Claras, Breves, and Estrela deposits, which formed during the Paleoproterozoic (Silva and Villas 1998; Tallarico et al. 2004; Botelho et al. 2005; Xavier et al. 2012).

IOCG-type deposits (Hitzman et al. 1992; Williams et al. 2005) have become prime targets for mineral exploration worldwide because they commonly show high ore grade and tonnage. Classic examples are the Olympic Dam and Ernest Henry deposits in Australia or Candelaria and Punta del Cobre deposits in Chile. Although proposed as a new genetic class of deposits (Hitzman et al. 1992), there is no consensus regarding the geological environment where they form and the sources of fluids, metals, and sulfur.

Regarding the Carajás IOCG deposits, there is much debate about how many Cu–Au mineralization events occurred in Archean-Proterozoic times, the simultaneity of the sulfide deposition in deposits with similar mineralization styles, the origin of high-salinity fluids, the age of mineralization, and the role played by granitic intrusions in the deposit genesis (Lindenmayer 1990; Lindenmayer et al. 2005; Villas and Santos 2001; Requia et al. 2003; Tallarico et al. 2005; Villas et al. 2005, 2006; Chiaradia et al. 2006; Dreher et al. 2008; Monteiro et al. 2008; Carvalho 2009; Xavier et al. 2008, 2010, 2012; Torresi et al. 2012; Moreto et al. 2013). Despite the advances in the knowledge of these deposits, several questions remain unanswered. The metallogenetic study of the Cu–Au Visconde deposit presented here provides insights to help solving some of those controversial topics, especially the nature of the mineralizing fluids and the temporal relationships between the ore formation and the granite emplacement.

The Visconde deposit (20–50 Mt at 1.0 % Cu, 0.28 g/t Au; Benevides Aires, personal communication) is one of the satellite ore bodies of the large Sequeirinho/Sossego deposit located approximately 15 km to the west. Recent studies (Craveiro 2011; Craveiro et al. 2012) have shown that, with respect to the stages and types of alteration, styles of mineralization, and fluid properties, the Visconde deposit is very similar to other Archean Cu–Au deposits of Carajás, especially those located near the boundary between the southern edge of the Carajás domain and the Transition domain, namely the Bacaba, Bacuri, Castanha, Alvo 118, Cristalino, Jatobá, and Sequeirinho/Sossego deposits (Fig. 1). To contribute to understanding of the genesis of the Visconde deposit, this study attempts to define the likely sources of the hydrothermal fluids based on stable isotope (O, H, and S) and fluid inclusion data, in addition to constrain the age of mineralization (Pb isotope).

Materials and methods

Core samples from eight boreholes drilled in the Visconde deposit area were studied petrographically, some with scanning electron microscopy coupled with energy dispersive X-ray spectrometry (EDS), at the Geosciences Institute of the Federal University of Pará (IG-UFPA).

For stable isotope analysis, pure mineral fractions were separated manually with the aid of a binocular lens from ground rock samples. These fractions consisted of silicates (32), oxides (4), and sulfides (12). Analyses were performed on albite, magnetite, quartz, and tourmaline (oxygen), actinolite, biotite, chlorite, and epidote (oxygen and hydrogen), chalcopyrite and bornite (sulfur). The isotopic composition of oxygen in silicates (except albite) was determined at the Center for Granite Research -Stable Isotope Laboratory (NEG-LABISE) of the Federal University of Pernambuco. Hydrogen in silicates, oxygen in magnetite and albite, and sulfur in sulfides were determined at the Queen's Facilities for Isotope Research (QFIR) at Queen's University (Canada). The BrF5 method of Clayton and Mayeda (1963) was used to extract oxygen. For hydrogen extraction the procedures followed those described in Kyser and Kerrich (1991). Stable isotope measurements were made using a Thermo-Finnigan Delta V Advantage (LABISE) and a Finnigan MAT 252 mass spectrometer (QFIR), and the results are expressed in the conventional delta per mil notation (δ, ‰). The oxygen and hydrogen isotopic compositions are reported in relation to Vienna Standard Mean Ocean Water (VSMOW) and the sulfur values in relation to Vienna Canyon Diablo Troilite (VCDT).

Fluid inclusion studies were carried out on five doubly polished thin sections prepared from core samples of three drill-holes (VISD-FD 35, VISD-FD 36, and VISD-FD 37) representing the altered granite, the breccia matrix and veins that crosscut the altered gabbro/diorite and metadacite. The studied inclusions were trapped in quartz, scapolite, apatite and calcite. Approximately 500 phase change temperatures were measured in tens of inclusions using a LINKAM THMS600 heating-freezing stage coupled to a conventional petrographic microscope at the Metallogenesis Laboratory of the Geosciences Institute of the Federal University of Pará (UFPA). Fluid compositions were estimated from eutectic

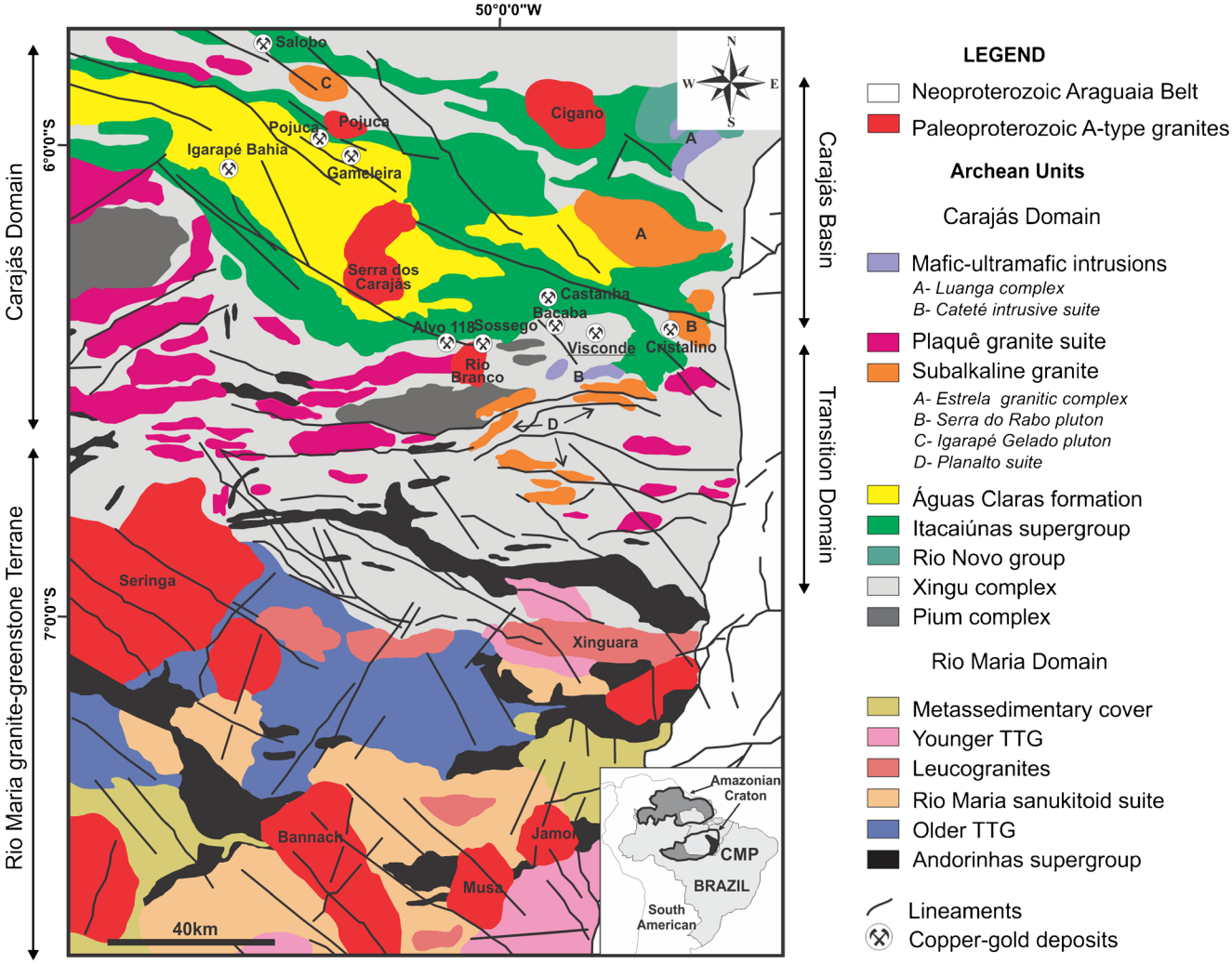

Fig. 1 Geological map of the CMP with the location of the Visconde and other cupro-auriferous deposits (compiled from DOCEGEO 1988; Gomes and Dall'Agnol 2007; Feio et al. 2012)

temperatures obtained experimentally in simple chemical systems by Borisenko (1977) and Davis et al. (1990).

The geochronological analyses were carried out at the Laboratory of Isotope Geology (Pará-Iso), IG-UFPA. Lead total digestion and leaching methods were used on chalcopyrite ore samples to date the mineralization. The experimental procedure followed the techniques described in Galarza et al. (2008) and Romero et al. (2013). During the total digestion, ≈100 mg of chalcopyrite underwent cold acid attack, and for the leaching procedure, 400 mg were progressively attacked by hot acids, and the resulting solutions were collected in six different steps (L1 to L6). Specific mixtures of tri-distilled HCl, HNO_3, and HBr were employed in both methods. Lead was separated by ion-exchange chromatography using an Eichrom® Sr 50–100 μm resin. The lead isotopic ratios were measured using a Thermo-Finnigan Neptune ICP-MS and corrected for mass discrimination by exponential law using the $^{205}Tl/^{203}Tl$ ratio. The total Pb blank of the analytical procedure ranged from 0.33 to 1.50 ng. Pb–Pb isochron ages were calculated with the ISOPLOT software (v.3.68) of Ludwig (2008). The errors on lead isotopic ratios were quoted at a 95 % confidence level.

Dating of a granitic body with no evidence of mineralization was accomplished by the Pb-evaporation method on zircon monocrysts (Kober 1986, 1987). Different size fractions of zircon grains were obtained by sieving and heavy liquid separation, but only those between 0.075 and 0.180 mm provided suitable grains for analysis. The experimental procedures, lead isotopic determinations, and age calculations are described in detail in Klötzli (1997) and Barreto et al. (2013). The analyses were performed on a TIMS Finnigan MAT 262 mass spectrometer at increasing temperature steps of 1450, 1500, and 1550 °C, with five blocks in each step. Ages were obtained using the weighted mean of $^{207}Pb/^{206}Pb$ ratios of each block, the most reliable values being those yielded at the highest temperature steps. The ISOPLOT software (v.3.68) of Ludwig (2008) was used for age calculations.

Regional geological setting

The CMP lies within the Archean southern Amazon Craton (Fig. 1). Two tectonic blocks are distinguished in the CMP: the southern Rio Maria Granite-Greenstone Terrane and the northern Carajás Domain. Given that the boundaries between these two tectonic blocks are not well defined, Dall'Agnol et al. (2006) proposed the existence of a Transition Domain, assumed to be an extension of the Rio Maria terrane intensely affected by the Neoarchean magmatic and tectonic events recorded in the Carajás Domain.

The Mesoarchean Rio Maria terrane consists of rocks with ages between 2.97 and 2.87 Ga, which comprise the greenstone-type sequences of the Andorinhas Supergroup and various granites, including trondhjemite-tonalite-granodiorite (TTG) series, Mg-rich granites (Rio Maria sanukitoid suite; Oliveira et al. 2009) and leucogranites (Dall'Agnol et al. 2006; Feio et al. 2012).

The Carajás Domain is largely made up of metavolcanic-sedimentary and meta-sedimentary rocks that were originally deposited in the intracratonic Carajás basin (Gibbs et al. 1986). The basin oldest unit is represented by the mafic-ultramafic rocks, iron formations, and schists of the Rio Novo Group (>2.76 Ga). The overlying Itacaiunas Supergroup (2.76–2.73 Ga) comprises the Igarapé Salobo, Igarapé Bahia, Grão Pará, Igarapé Pojuca, and Buritirama groups, which show different metamorphic grades (greenschist to amphibolite facies) and varying deformation intensities related to the Itacaiúnas transpressive ductile shear zone (Pinheiro and Holdsworth 2000). Amphibolites, paragneisses, metavolcanic rocks, pelitic schists, meta-arkoses, and iron formations are common lithotypes and host most of the Fe, Cu, and Au deposits of Carajás.

The Rio Novo Group rocks are cut by the mafic-ultramafic-layered Luanga Complex (2.76 Ga; Machado et al. 1991) and by metaluminous, alkaline granites that transect units of the Itacaiunas supergroup. The syn- to late-tectonic granites are represented by the Estrela, Serra do Rabo, Cristalino, and Igarapé Gelado intrusions, with ages ranging from 2.76 to 2.73 Ga (Huhn et al. 1999; Barros et al. 2001; Sardinha et al. 2006). The Igarapé Salobo group hosts the ca. 2.5 Ga Itacaiunas and Old Salobo granites (Machado et al. 1991; Souza et al. 1996).

These older rocks are unconformably overlain by the siliciclastic and minor volcaniclastic rocks of the Aguas Claras Formation, with ages varying from 2.68 to 2.64 Ga (Nogueira et al. 1995; Dias et al. 1996; Trendall et al. 1998).

In the Transition domain, the oldest rocks belong to the Pium Complex, which includes granulites formed at ~3.0 Ga and metamorphosed at 2.86 Ga (Rodrigues et al. 1992; Pidgeon et al. 2000), as well as diopside-norites dated at 2745±1 and 2744±1 Ma (Pb–Pb zircon; Santos et al. 2013a, b).The Xingu Complex consists mainly of undifferentiated granites, gneisses and migmatites associated with subordinate amphibolites, metamorphosed at ca. 2.86 Ga (Machado et al. 1991).

A few intrusive suites have been recognized in the Transition Domain. The Neoarchean Plaquê and Planalto suites consist of numerous E-W-oriented granitic bodies, the former (~2.73 Ga, Avelar et al. 1999) being composed of metaluminous to peraluminous, alkaline to calc-alkaline lens-shaped intrusions (Macambira et al. 1996). The latter (2.74–2.73 Ga; Huhn et al. 1999; Sardinha et al. 2004; Feio et al. 2012) comprise subalkaline, metaluminous to weakly peraluminous stocks. The Cateté intrusive suite is represented by mafic-ultramafic intrusions. Geochronological data are only available from a gabbro (Serra da Onça intrusion) and yield a Sm–Nd isochronic age of 2378±55 Ma (Macambira and Tassinari 1998) and a SHRIMP U–Pb age on zircon of 2766±6 Ma (Lafon et al. 2000).

After a long period with no rock record, a magmatic episode took place at 1.88 Ga throughout the CMP during an extensive or transtensive event (Pinheiro and Holdsworth 2000). Several isotropic A-type granites were then emplaced, such as the Cigano, Jamon, Bannach, Musa, Pojuca, Seringa, Serra dos Carajás, and Rio Branco intrusions, some of them mineralized with Cu and Au (Machado et al. 1991; Dall'Agnol et al. 2005; Santos et al. 2013a, b).

The Visconde Cu–Au deposit

The Visconde deposit (Craveiro et al. 2012; Fig. 2) is located within a regional WNW-ESE-trending shear zone that is approximately 60 km long at the contact between a metavolcanic-sedimentary sequence of the Itacaiunas supergroup (Grão Pará Group?) and the basement (Xingu Complex and other granitic units). The Cu–Au Bacaba, Castanha, Alvo 118, Cristalino, Jatobá, and Sossego deposits also occur along that shear zone. The Sossego deposit is composed of the Sequeirinho, Sossego, Pista, Baiano, and Curral ore bodies, with the first two representing more than 85 % of the ore reserves.

The Visconde deposit is hosted by felsic metavolcanic rocks, the Serra Dourada granite, gabbros/diorites and, to a lesser extent, ultramafic rocks (Fig. 3). These rocks are hydrothermally altered and crosscut by mylonitic zones, along which abundant hydrothermal minerals formed, especially biotite. The felsic metavolcanic rocks, described as metadacites according to Craveiro et al. (2012), are gray colored and fine grained and show isotropic to foliated varieties. When foliated, they display fine alternating bands composed of quartz, plagioclase, muscovite or biotite, and/or hornblende. The Serra Dourada granite (2,60±22 Ma, Moreto et al. 2011) is coarse-grained, isotropic, although incipiently foliated in places, and grayish to pinkish in color.

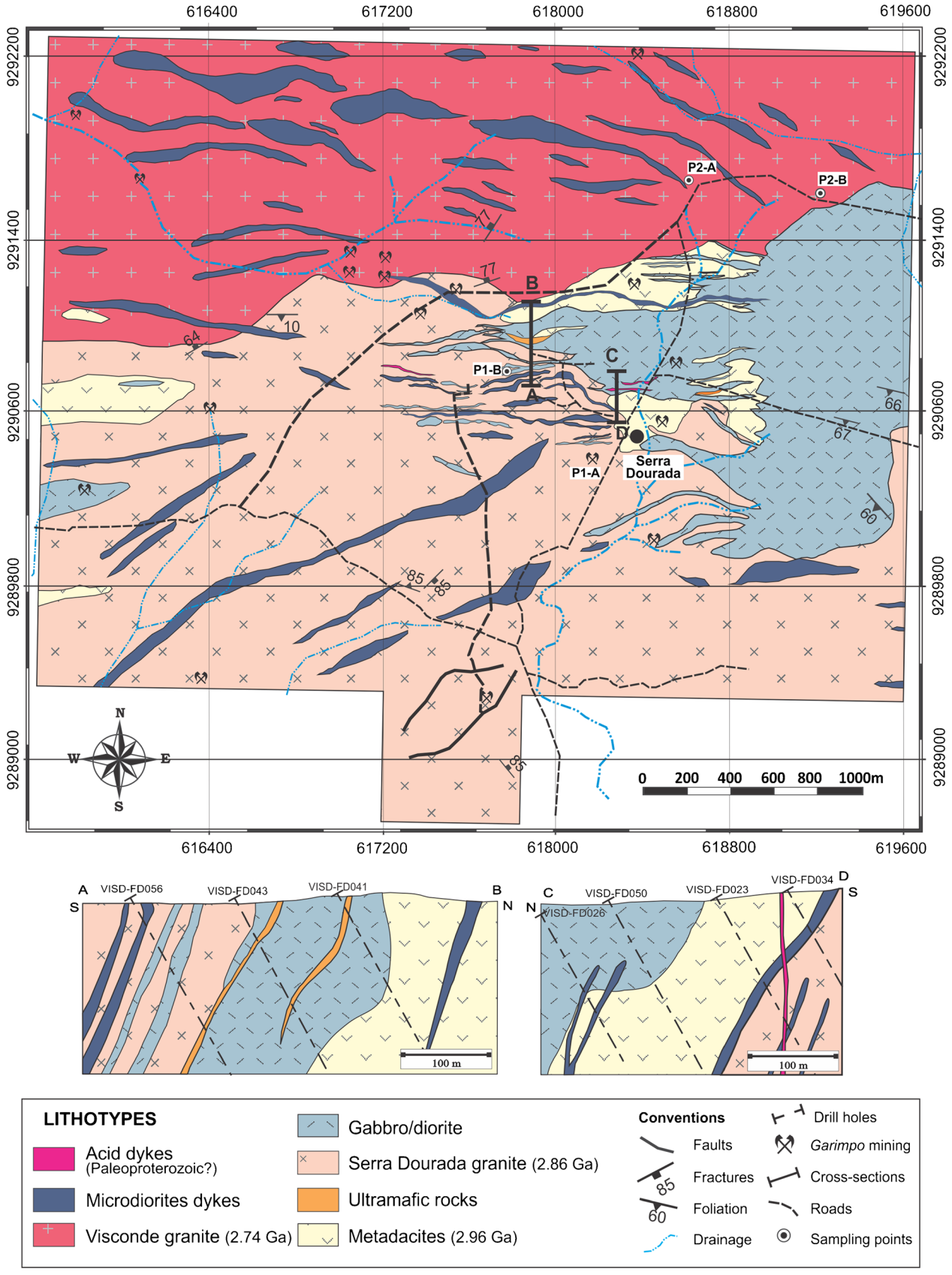

Fig. 2 Geological map (**a**) and a N-S cross-section (**b**) of the Visconde deposit (modified from VALE, unpublished, 2003)

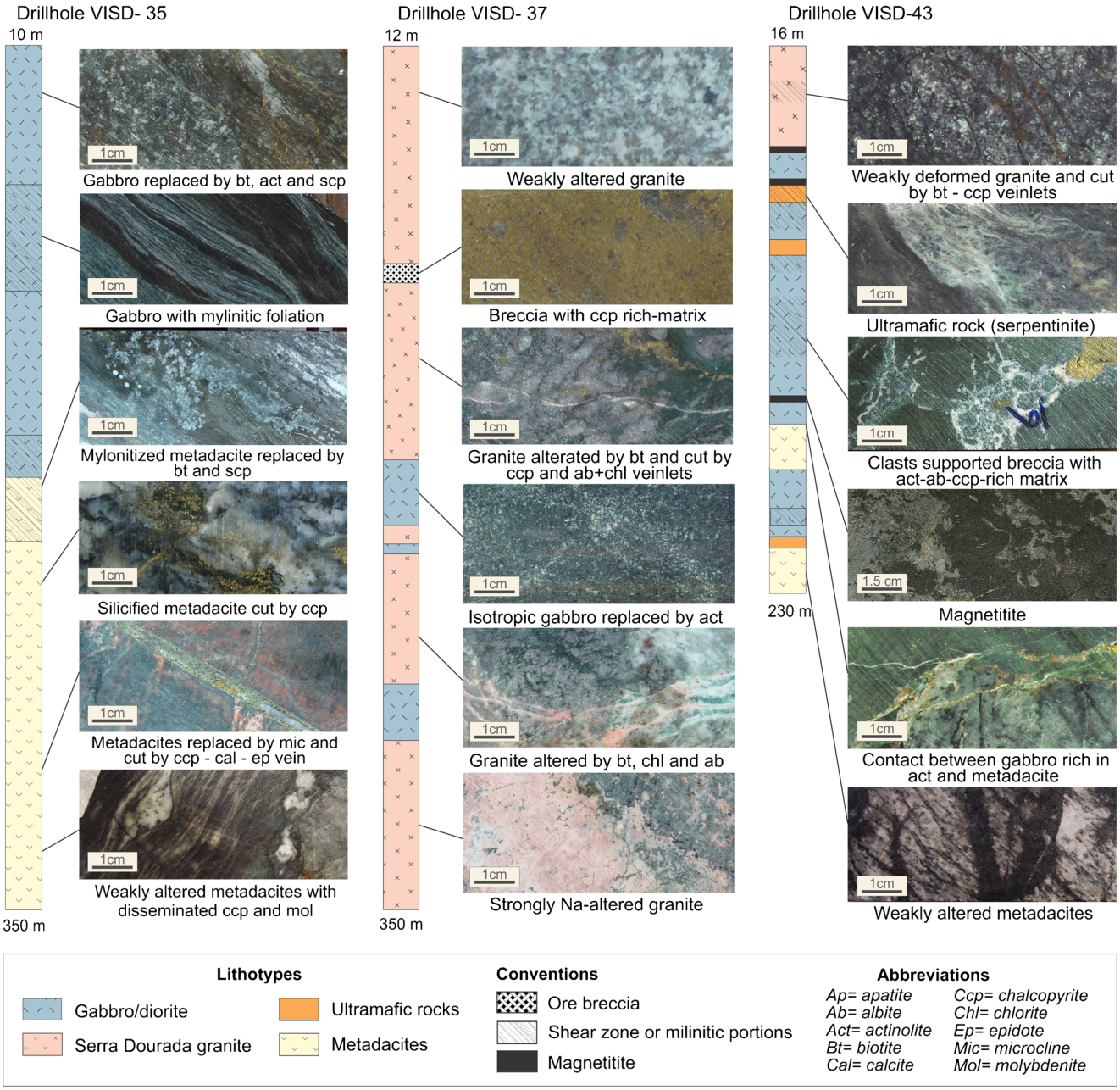

Fig. 3 Main features of altered and mineralized rocks of the Visconde deposit. Simplified description of representative drill cores (VSD-35, VSD-35, and VSD-43)

Quartz, plagioclase, and K-feldspar are the main mineral constituents, giving the rock a monzogranitic to granodioritic composition with calc-alkaline affinity. This intrusion bears evidence of Na metasomatism indicated by the common occurrence of chessboard albite (Craveiro et al. 2012; Feio et al. 2013).

Gabbro/diorites occur as stocks and dikes, and are apparently intrusive in both the metadacites and the Serra Dourada granite. These gabbro/diorites are medium-grained and, when less altered, display primary relict features such as sub-ophitic texture and straight contacts among plagioclase, Mg hornblende, or quartz crystals, in addition to primary magnetite crystals with exsolved ilmenite lamellae.

Ultramafic lenticular bodies occur in some gabbros and the Serra Dourada granite, being represented by magnesite- and talc-rich serpentinites, with lesser amounts of pentlandite, Ni-bearing chalcopyrite and magnetite. Most rocks are strongly oriented in the E-W direction and steep-dipping in response to the development of a ductile–brittle to brittle shear zone in the Neoarchean (2.76–2.65 Ga; Pinheiro and Holdsworth 2000).

The Visconde granite

A slightly altered, highly fractured (Fig. 4a), but nonmineralized granitic body, referred to here as the Visconde granite, occurs in the northern part of the deposit area (Fig. 2). It is reddish pink, isotropic, medium to coarse grained, and displays a heterogranular texture, locally with graphic intergrowth (Fig. 4b, c). Microcline, quartz, plagioclase, and biotite are the major minerals, with a modal composition of syenogranite. Microcline crystals are coarse and commonly perthitic. Quartz crystals are anhedral to subhedral, some with weak undulose extinction. Plagioclase occurs as exsolution lamellae in microcline and as subhedral crystals, some showing kink bands and microfractures. Most biotite occurs interstitially as isolated flakes. Zircon is the main primary accessory mineral, whereas minor sericite, chlorite, epidote, and clay minerals represent the secondary phases, generally concentrated near fractured zones (Fig. 4b, d).

This body was initially described as a 1.88 Ga anorogenic granite (Vale 2003). More recently, based on petrographic data, it was tentatively correlated to the Planalto suite (Feio et al. 2012), with age determined at 2.74 Ga (Huhn et al. 1999; Sardinha et al. 2004; Feio et al. 2012). However, the age of the granite remains an open question. Despite having fractured zones potentially favorable to fluid circulation, this granite shows no signs of alkali-metasomatism or mineralization, suggesting that its emplacement took place after the Visconde mineralizing event.

Hydrothermal alteration and mineralization

The hydrothermal alteration evolved in various stages and was largely controlled by tectonic evolution from a ductile to a brittle regime. During the first stage of the early sodic-calcic alteration, the rock underwent a pervasive replacement of primary mineral assemblages. Chessboard albite in the Serra Dourada granite (Fig. 5a) and marialitic scapolite that formed in the gabbros/diorites at the expense of the plagioclase (Fig. 5b) are typical minerals of this stage. Early veins (albite-epidote, scapolite-tourmaline, tourmaline-quartz, and actinolite; Fig. 5c, d) and aggregates of actinolite, locally associated with magnetite (with fine inclusions of ilmenite and rutile; Fig. 6g, h), are the most conspicuous early hydrothermal products. Disseminated chalcopyrite and pyrite are common. More magnetite precipitated later on, locally forming magnetitites. The potassic stage developed next and characteristically produced biotite (Fig. 5e) and K-feldspar. In highly deformed rocks, biotite is so abundant and the mylonitic foliation so pronounced that they resemble a schist (Fig. 5e). In the deformed ultramafic rock lenses, talc and magnesite also formed in addition to biotite (Fig. 5g). The corresponding alteration assemblages also include quartz, allanite, magnetite, chalcopyrite, and molybdenite. Next abundant sulfides

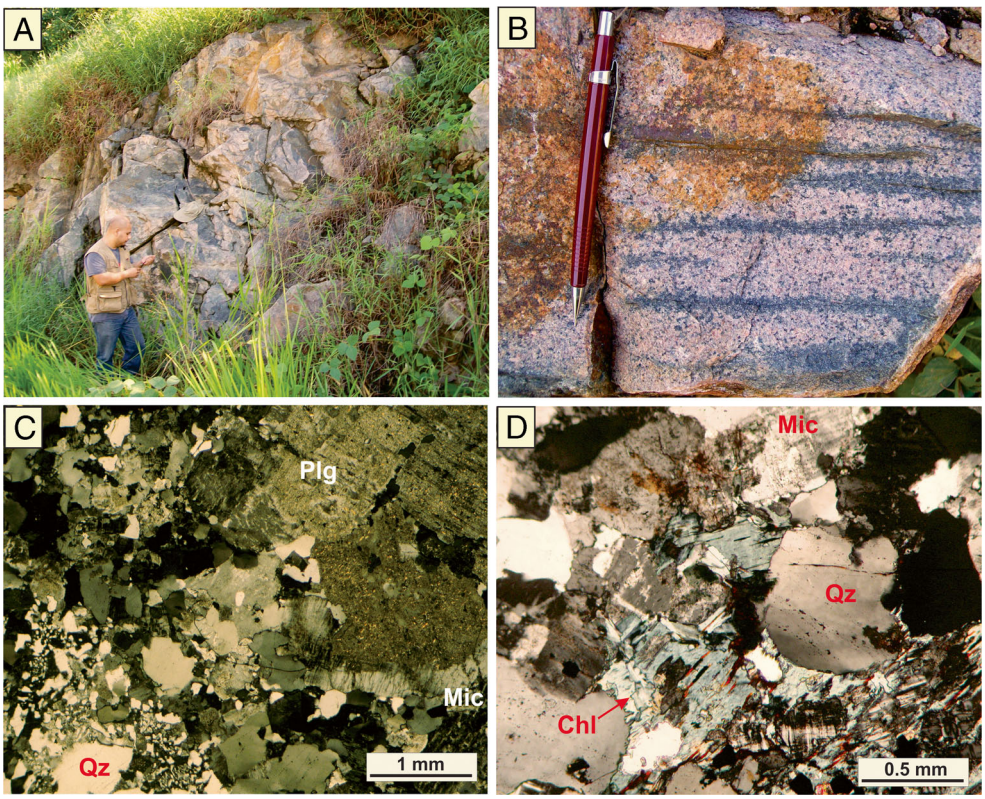

Fig. 4 Features of the Visconde granite. **a** Photograph of an outcrop located at the km 7 along the Sossego mine road. **b** The *pinkish gray color* of the Visconde granite contrasting with the *dark greenish color* of the chloritization halos along the fractures.; **c** Photomicrograph of the hypidiomorphic granular texture of the rock with a local graphic intergrowth. **d** Photomicrograph of chlorite lamellas partially replacing microcline. Chlorite is one of the most abundant hydrothermal alteration product in the Visconde granite. *Chl* chlorite, *Mic* microcline, *Plg* plagioclase, *Qz* quartz

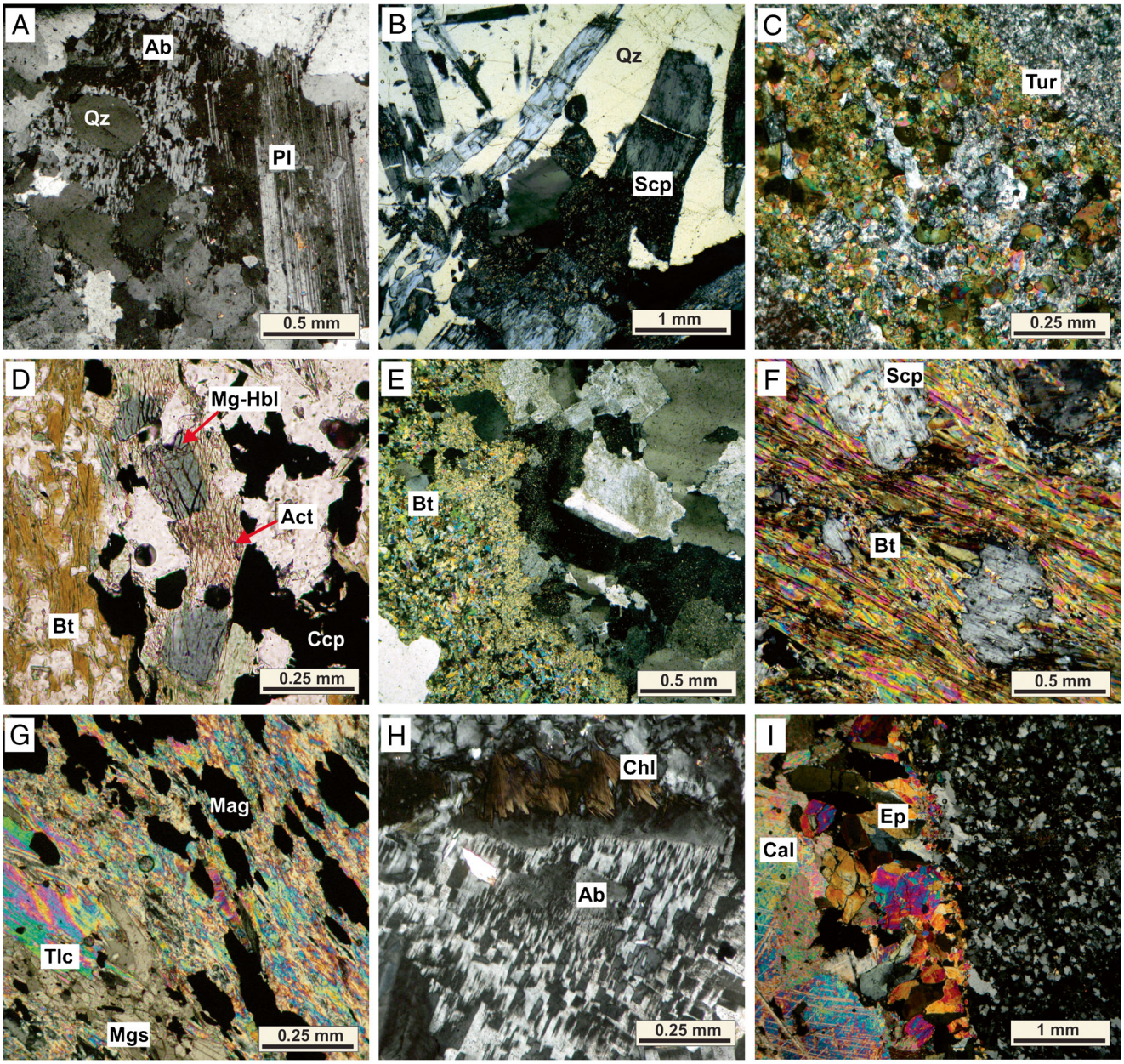

Ab = albite; Act = actinolite; Bt = biotite; Cal = calcite; Ccp = chalcopyrite; Chl = chlorite; Ep = epidote; Mag = magnetite; Mg-Hbl = Mg-Hornblende; Mgs = magnesite; Pl = plagioclase; Qz = quartz; Scp = scapolite; Tlc = talc; Tur = tourmaline.

Fig. 5 Photomicrographs of common alteration assemblages at the Visconde deposit. **a** Chessboard albite in the Serra Dourada granite rocks. **b** Scapolite aggregate crosscut by a quartz vein. **c** Early tourmaline-bearing vein hosted by metadacite. **d** Mg hornblende partially replaced by actinolite (in a biotite-rich altered diorite). **e** Biotitization zone in the Serra Dourada granite. **f** Gabbro/diorite affected by mylonitization and replaced by scapolite and biotite. **g** Mylonitized ultramafic rock with talc, magnesite, and magnetite. **h** Chessboard albite and chlorite in a millimeter-thick late vein. **i** Epidote- and calcite-bearing vein in a metadacite

(chalcopyrite>>bornite) precipitated, while a new episode of sodic-calcic and magnesian alteration occurred in the outer zones, with albite, epidote, chlorite, calcite, and minor fluorite filling fracture-controlled veins and veinlets (Fig. 4h, i). The hydrothermal history ended with a calcic-magnesian alteration characterized by the precipitation of chlorite, calcite and local gypsum or hematite in veinlets and/or breccias (Fig. 6i).

The ore occurs as tectonic breccias, veins, veinlets and disseminations (Fig. 6a, b). The breccias form bodies that transect the potassic alteration zones (Fig. 6c–f). These breccias consist of clasts of hydrothermally altered rocks

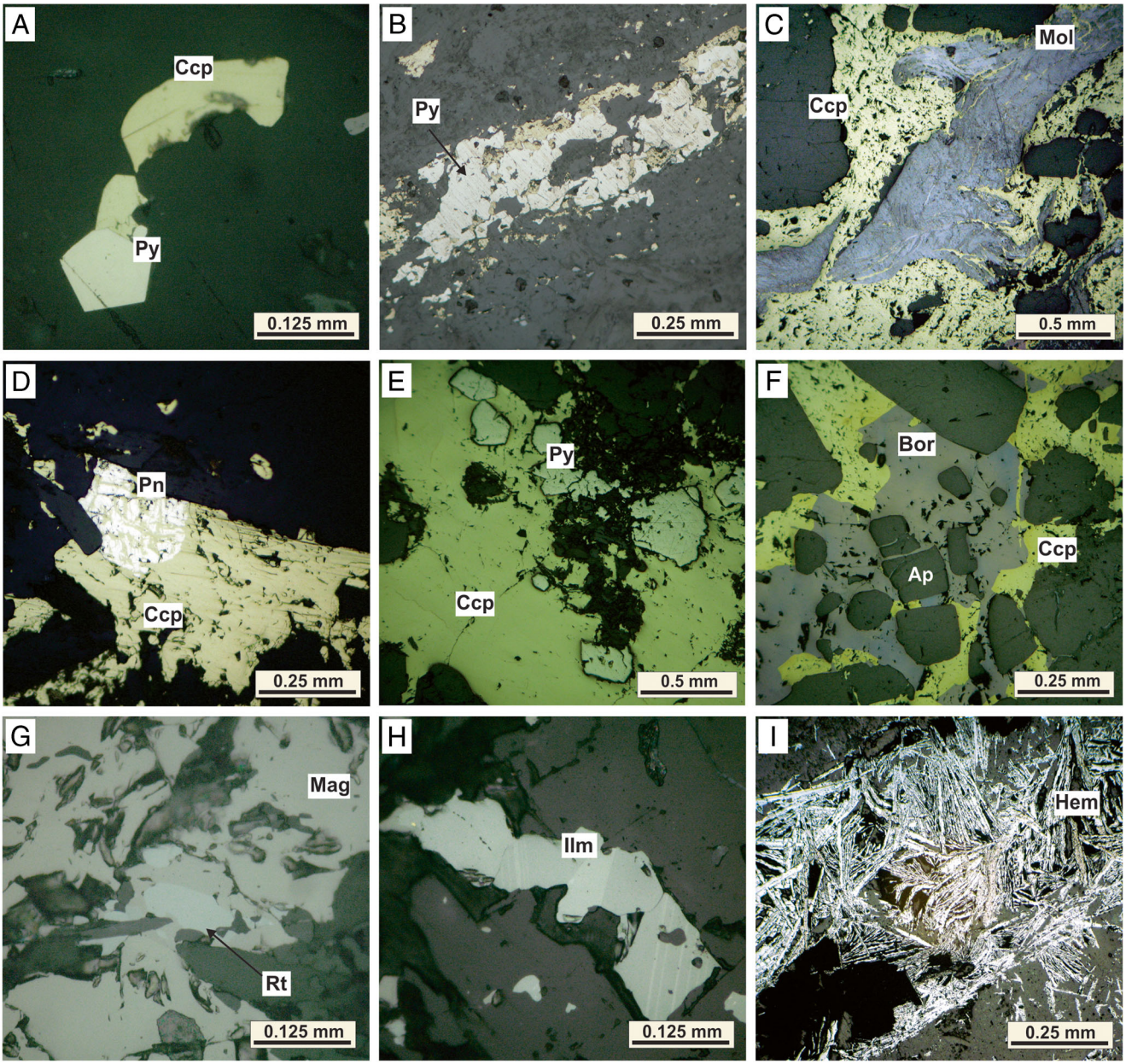

Ap = apatite; Bor = bornite; Ccp = chalcopyrite; Hem = hematite; Ilm = Ilmenite; Mag = magnetite; Mol = molybdenite; Pn = pentlandite; Py = pyrite; Rt = rutile.

Fig. 6 Textural features of the main sulfides and oxides at the Visconde deposit. **a** Chalcopyrite and pyrite disseminations in gabbro/diorite. **b** Chalcopyrite and pyrite along a mylonitic foliation plane developed in metadacite. **c** Breccia matrix containing molybdenite partially replaced by chalcopyrite (in gabbro/diorite). **d** Early pentlandite crystal replaced by chalcopyrite along a cleavage plane. Gabbro/diorite. **e** Pyrite clasts cemented by chalcopyrite-rich breccia matrix, in Serra Dourada granite. **f** Apatite clasts immersed in a chalcopyrite- and bornite-rich breccia matrix, in gabbro/diorite. **g** Rutile inclusions in a magnetite crystal, in gabbro/diorite. **h** Disseminated ilmenite close to a magnetitite body, in gabbro/diorite. **i** Needle-like hematite in a late vein cutting a rhyolite dyke

immersed in a matrix of sulfides (locally over 60 %), chiefly chalcopyrite, together with minor bornite, pyrite, chalcocite, covellite, and digenite. In veins and veinlets, the sulfides co-precipitated with sodic-calcic minerals. The paragenetic sequence in the Visconde deposit is summarized in Fig. 7.

Isotope geochemistry

Oxygen isotopes

$\delta^{18}O_{VSMOW}$ data from hydrothermal minerals representative of the different alteration stages recorded in the Visconde

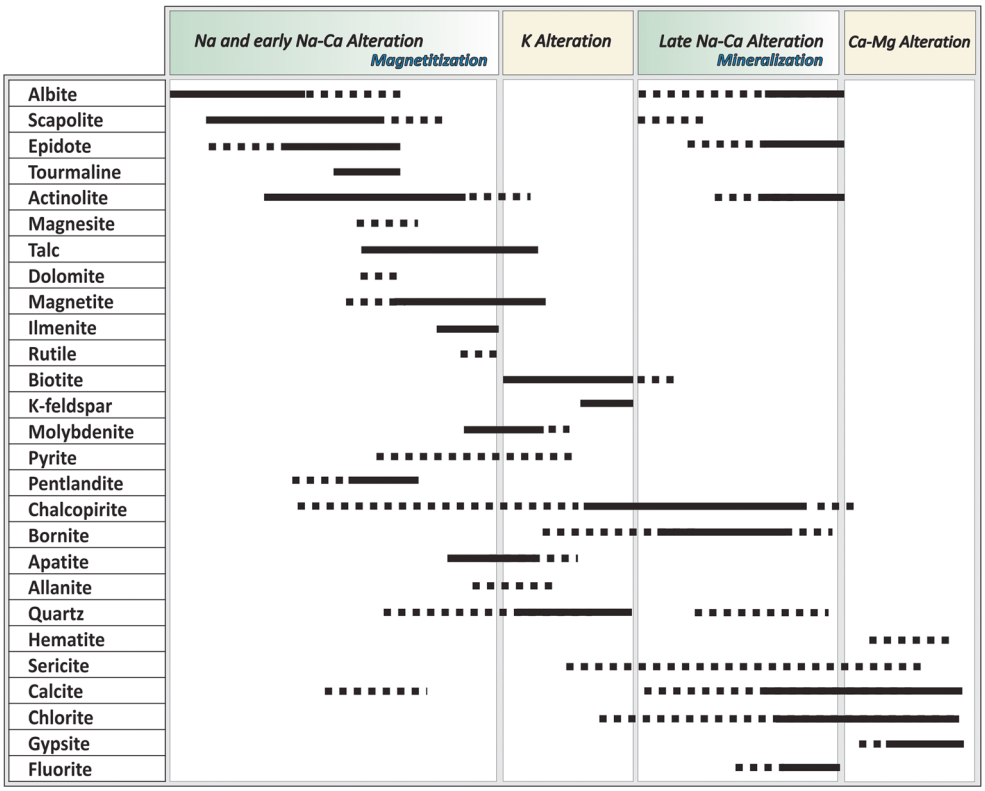

Fig. 7 Mineral paragenetic sequence of altered and mineralized rocks from the Visconde deposit

deposit are reported in Table 2. The measured $\delta^{18}O_{VSMOW}$ values in the silicates vary between +2.3 and +11.6‰, although for each mineral the range is narrow. The greatest variation is for chlorite (+2.3 to +5.1‰), though it does not reach 3‰. For magnetite, the values range from −1.3 to +0.5 ‰.

The formation temperatures of some mineral pairs (Table 1) were calculated based on oxygen isotope fractionation factors (Wenner and Taylor 1971; Matsuhisa et al. 1979; Zheng 1991, 1993). Mineral pairs were selected after careful petrographic examination to ensure textural equilibrium and, as much as possible, to have remained unaffected by subsequent alteration stages. The actinolite-magnetite pair from the early aggregates yielded the highest temperatures of 410± 21 °C, below the temperature of 470 °C obtained by fluid inclusion microthermometry in scapolite and quartz crystals that precipitated during the early sodic-calcic alteration (see below). A quartz-tourmaline pair from a vein formed during this same alteration stage yielded temperature of 355 °C, whereas the albite-epidote pair from a later vein, coeval with the main sulfide deposition, recorded a lower temperature of 237 °C.

Hydrogen isotopes

δD_{VSMOW} values from hydroxyl-bearing silicates (actinolite, biotite, epidote, and chlorite) are presented in Table 2. The values for actinolite (early sodic-calcic alteration) range from −47 to −61‰ and coincide partly with those for biotite from the potassic zones (−54 to −66‰). Chlorite and epidote (later stages) yielded values from −63 to −66 and from −18 to −49 ‰, respectively. Except for epidote, the δD_{VSMOW} results for the other minerals overlap largely.

Table 1 Temperatures estimated from oxygen isotopic composition of hydrothermal minerals from the Visconde deposit

Alteration stage	Alteration type	Temperature
Regional early sodic alteration	Sodic alteration[a]	470 °C
Early sodic-calcic alteration	Actinolitite	Act-mag pair (431 °C)
		Act-mag pair (389 °C)
		Mean (410±21 °C)
	Silicification	Qz-tur pair (355 °C)
Mineralization and late sodic-calcic alteration	Chloritization[b]	285±7 °C
	Late vein and veinlets	Ab-ep pair (240 °C)
		Ab-ep pair (233 °C)
		Ab-cl pair (218 °C)
		Mean (229±11 °C)

Oxygen isotope fractionations: magnetite–H_2O (Zheng 1991); tourmaline-H_2O, albite–H_2O, actinolite–H_2O, and epidote–H_2O (Zheng 1993); quartz–H_2O (Matsuhisa et al. 1979); and chlorite–H_2O (Wenner and Taylor 1971)

[a] Fluid inclusion data in scapolite

[b] Chlorite geothermometer (Craveiro et al. 2012)

Isotopic composition of the hydrothermal fluids

The temperatures calculated for each alteration stage were used to estimate the hydrogen and oxygen isotopic composition of the fluids (Table 2), using the fractionation factors for actinolite-H_2O, magnetite-H_2O, quartz-H_2O, tourmaline-H_2O, biotite-H_2O, epidote-H_2O, albite-H_2O, and chlorite-H_2O (Wenner and Taylor 1971; Bottinga and Javoy 1973; Suzuoki and Epstein 1976; Matsuhisa et al. 1979; Graham et al. 1980, 1984; Zheng 1991, 1993).

For the early sodic-calcic alteration (actinolite and magnetite), which recorded temperatures of 410±21 °C, the $\delta^{18}O_{H_2O}$ and δD_{H_2O} values fall within the ranges +5.6±0.2 to +9.4±0.1 and −32 to −18‰, respectively. Lower $\delta^{18}O_{H_2O}$ values (+3.3 to +5.7‰) were obtained for the fluids in equilibrium with tourmaline and quartz (at 355 °C). The biotite formation temperature is uncertain. Nevertheless, the fluid isotopic

Table 2 Isotopic composition ($\delta^{18}O_{VSMOW}$ and δD_{VSMOW}) of silicate minerals, magnetite, and fluid of the Visconde deposit (values in ‰)

Sample	Description	Mineral	$\delta^{18}O_{min}$	T (°C)	$\delta^{18}O_{H_2O}$	δD_{min}	δD_{H_2O}
19/43	Actinolitite	Act	+6.7	410±21	+7.9±0.1		
5/43	Mag+Act aggregate	Act	+6.8	410±21	+8.0±0.1		
13/43	Mag+Act aggregate	Act	+8.2	410±21	+9.4±0.1	−49	−20
5/32	Actinolitite cut by ccp vein	Act	+6.3	410±21	+7.5±0.2	−54	−25
F36-25m	Actinolitite	Act	+5.8	410±21	+7.0±0.2	−61	−32
6/43	Actinolitite	Act	+6.2	410±21	+7.4±0.1	−61	−18
5/43	Mag+Act aggregate	Mag	−0.1	410±21	+6.7±0.2		
13/43	Mag+Act aggregate	Mag	−1.0	410±21	+5.8±0.2		
F36-171	Magnetitite	Mag	+0.5	410±21	+7.4±0.2		
F36-224	Magnetitite	Mag	−1.3	410±21	+5.6±0.2		
P2-2	Qz±ccp veinlet	Qz	+10.4	355	+5.3		
13/32	Early qz+tur vein	Qz	+10.1	355	+5.0		
15/32	Early qz+tur vein	Qz	+9.3	355	+4.2		
19/43	Early qz vein	Qz	+9.9	355	+4.7		
23,5/93	Early qz vein	Qz	+9.8	355	+4.6		
10/50	Clasts of tur ccp-matrix breccia	Tur	+5.0	355	+3.3		
15/32	Early qz+tur vein	Tur	+7.3	355	+5.6		
10/39	Macrocrystals of tur	Tur	+7.4	355	+5.7		
13/32	Early qz+tur vein	Tur	+7.1	355	+5.4		
10/39	Bt along mylonitic foliation	Bt	+4.9	355	+6.7	−57	−3
5/32	Iintersticial Bt in actinolitite	Bt	+5.2	355	+6.9	−66	−12
19/43	Iintersticial Bt in actinolitite	Bt	+5.1	355	+6.9	−66	−4
24/37	Granite altered by bt	Bt	+3.0	355	+4.8		
23.5/43	Bt along mylonitic foliation	Bt	+5.4	355	+7.2	−58	−12
16/37	Late ep+ab vein	Ep	+3.5	229±11	+0.7±0.3	−49	−26±4
F36-244	Late ep+ab+mag vein	Ep	+4.5	229±11	+1.7±0.3	−18	+6±4
27/32	Late ep+cal+ab+ccp vein	Ep	+4.0	229±11	+1.3±0.3	−29	−5±4
23/37	Late ep vein	Ep	+3.6	229±11	+0.8±0.4	−31	−8±5
F36-244	Late ab+ep+ccp vein	Chl	+4.1	229±11	+2.6±0.3	−66	−28
23/37	Late chl vein	Chl	+2.3	229±11	+0.9±0.2	−66	−27±1
16/37	Late chl veinlets	Chl	+3.9	229±11	+2.4±0.2	−63	−24±1
24/32	Late chl vein	Chl	+5.1	229±11	+3.7±0.2		
27/32	Late chl vein	Chl	+4.0	229±11	+2.6±0.2		
23/37	Late ab+ep+ccp vein	Ab	+6.0	229±11	−1.3±0.4		
F36/244	Late ep+cal+ab+ccp vein	Ab	+6.9	229±11	−0.4±0.4		
16/37	Late ab+ep vein	Ab	+11.6	229±11	+4.4±0.4		

Ab albite, *Act* actinolite, *Bt* biotite, *Cal* calcite, *Chl* chlorite, *Ep* epidote, *Mag* magnetite, *Tur* tourmaline, *Qz* quartz

composition was also calculated at 355 °C because, within the paragenetic sequence, it is the closest temperature suggested for the biotite appearance. Thus, fluids related to the potassic alteration show $\delta^{18}O_{H_2O}$ values between +4.8 and +7.2‰ and δD_{H_2O} values spread over the −12 to −3‰ interval. At the final alteration stages, the temperature was approximately 229 ±11 °C and the fluids became ^{18}O depleted ($\delta^{18}O_{VSMOW}$= −1.3±0.4 to +4.4±0.4‰) but highly variable in δD_{VSMOW} (−28 to −24‰ for chlorite and −26 to +5‰ for epidote).

Sulfur isotopes

Sulfur isotope compositions ($\delta^{34}S_{VCDT}$) were determined in chalcopyrite and bornite samples (Table 3). The results show narrow variation (+0.5 to +3.4‰), the higher values tending to be recorded in late vein and breccia sulfides. Disseminated and early vein sulfides reveal compositions slightly above zero (+0.5 to +1.5‰) whereas one sample (cpy 24–32) has a negative value (−1.2‰). Although chalcopyrite and bornite from sample 24–32 were apparently in equilibrium, attempts to calculate the formation temperature returned unrealistic values.

Fluid inclusion microthermometry

Data from fluid inclusions in hydrothermal minerals revealed three distinct aqueous fluids characterized as the following chemical systems: H_2O–NaCl–$CaCl_2$±$MgCl_2$ (fluid 1), H_2O–NaCl–$FeCl_2$±$MgCl_2$ (fluid 2), and H_2O–NaCl±KCl (fluid 3). Only found in secondary inclusions, fluids 2 and 3 seem to have circulated after the copper-gold mineralizing event and will not be discussed hereafter.

Fluid 1 was primarily responsible for the wall-rock alteration and mineralization. It was trapped in two-phase (L+V), three-phase (L+V+S) and rare multi-phase (L+V+S1+S2) fluid inclusions, as observed at room temperature, in quartz, scapolite, apatite, and calcite host minerals. Saturated inclusions, with daughter crystals, were not identified in carbonate. Quartz and calcite samples are from the altered granite (both hydrothermal and recrystallized magmatic grains) and the breccia matrix, respectively. In turn, scapolite and apatite samples are from veins that crosscut the gabbro/diorite and the metadacite, respectively. Those fluid inclusions occur individually or clustered along intra-granular trails, and tend to be preferentially located in the crystal cores, what allow them to be assumed primary or pseudosecondary in origin. Their shapes are mostly subrounded to irregular with dimensions that range from 2 to 15 μm and degree of filling fairly uniform (0.7 to 0.9). The daughter mineral in the three-phase inclusions is most likely halite, whose cube edges vary from 1 to 4 μm, seldom 7 μm. In the multi-phase inclusions, the other daughter mineral is probably hematite with size that does not exceed 3 μm. Figure 8 displays some morphological characteristics of the three- and two-phase inclusions trapped in a quartz and apatite crystals.

Cooling revealed that the eutectic temperatures range from −68 to −44 °C, but most measurements (85 %) fall between

Fig. 8 Photomicrographs and their respective sketches of fluid inclusions hosted by quartz (*A–C*) from the altered Serra Dourada granite and apatite (*D*) from a polyminerallic vein that crosscuts a metadacite. *A*, *A'* Hydrothermal quartz crystal containing inclusions that trapped fluid 1 and are clustered in small groups or along intra-granular trails. The inter-granular trails contain secondary inclusions (fluid 2 or 3). *B*, *B'* Three-phase primary fluid inclusions located at the right upper corner of the quartz crystal pictured in (*A*). *C*, *C'* An intra-granular trail defined by three- and two-phase fluid inclusions, both primary and pseudosecondary, developed in the *left lower corner* of the quartz crystal shown in (*A*). *D*, *D'* Trails of two-phase secondary (?) inclusions that follow basal cleavage planes of a crystal of apatite. Note an isolated primary three-phase fluid inclusion at the center of the figure

Table 3 Sulfur isotope composition ($\delta^{34}S_{CDT}$) of sulfides from the Visconde deposit (values in ‰)

Amostra	Descrição	Mineral	$\delta^{34}S_{min}$ (‰)
10/52	Ccp vein along mylinonitc foliation in metadacyte	Ccp	+1.5
2/35	Disseminated ccp in gabbro	Ccp	+0.9
5/32	Qz vein cutting actinolitite	Ccp	+2.2
F36-25	Early ccp vein in actinolitite	Ccp	+0.5
11/39	Bor vein in gabbro	Bn	+2.6
24/32	Late ccp+bor+ep+ab vein in metadacyte	Bn	+3.3
24/32	Late ccp+bor+ep+ab vein in metadacyte	Ccp	−1.2
14/37	Late ccp e chl vein in granite	Ccp	+2.9
23/37	Late ccp+ep+ab+chl vein in metadacyte	Ccp	+2.8
12/37	Ccp-matrix breccia in gabbro	Ccp	+3.4
10/50	Ccp-matrix breccia in gabbro	Ccp	+2.2
23.5/43	Bor-matrix breccia in gabbro	Bn	+2.5

Isotopic calculations are based on the fractionation factors of Ohmoto and Rye (1979)

Ab albite, *Act* actinolite, *Bn* bornite, *Ccp* chalcopyrite, *Chl* chlorite, *Ep* epidote, *Tur* tourmaline, *Qz* quartz

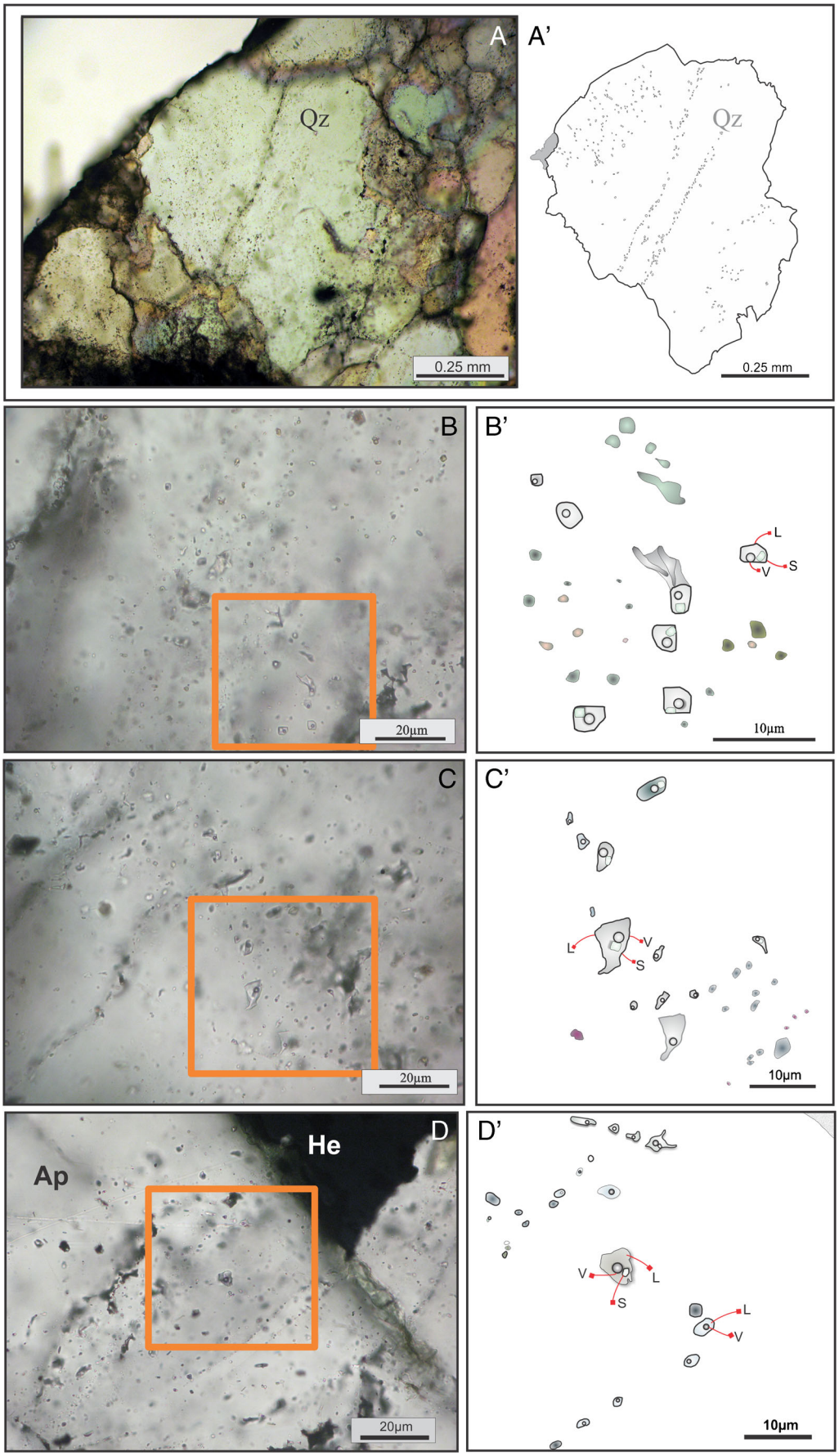
A
Qz
0.25 mm
A'
Qz
0.25 mm
B
20μm
B'
L
V
S
10μm
C
20μm
C'
L
V
S
10μm
D
He
Ap
20μm
D'
V
L
S
L
V
10μm

−58 and −50 °C. This may indicate that NaCl, $CaCl_2$, and $MgCl_2$ are the main solutes, although KCl is also assumed to have been an important component especially in the solutions that accounted for the potassic alteration. Ice melting temperatures for the unsaturated inclusions record values from −21 to −3 °C.

During heating, the three-phase inclusions homogenized into the liquid state by disappearance of the solid. In a few inclusion trapped in quartz, however, the gas bubble was the last phase to disappear. The multi-phase inclusions did not homogenize even at temperature as high as 600 °C (limit of the Linkam thermometric apparatus). Most likely they represent heterogeneous trapping, although the nondissolution of the solids could also be due to kinetic factors or leaking. All two-phase inclusions homogenized into the liquid state.

The homogenization temperatures (Th) cover a wide range (160–478 °C), the highest values corresponding to three-phase inclusions hosted by scapolite and quartz crystals, followed by three-phase inclusions trapped in apatite (355 to 412 °C). The temperature gap (~350–300 °C) may reflect incomplete sampling or the limited number of the analyses done. Below approximately 300 °C most Th record come from two-phase inclusions, including those trapped in calcite crystals, which have Th as high as 290 °C. As will be discussed later, at this stage the mineralizing fluid would have undergone significant dilution. Except for scapolite, whose fluid inclusions did not yield Th less than 190 °C, the other host minerals kept forming at least until ~150 °C.

From a paragenetic point of view, considering the minimum temperatures of trapping, the first generations of scapolite, quartz and apatite formed apparently in this order. Calcite came next after the hydrothermal system having experienced a temperature drop of ~200 °C.

Fluid salinities were estimated for unsaturated and saturated inclusions using the equations proposed by Bodnar (1993) and Sterner et al. (1988), respectively. The calculated values show also a wide variation (56 to 7 wt.% equiv. NaCl). As a rule, the lower the Th, the lower is the salinity, indicating that the fluid may have mixed with colder and less saline solutions as the hydrothermal system evolved.

Geochronology

Pb evaporation of zircon single crystals

The sample selected for dating the Visconde granite was medium grained, isotropic, devoid of fractures, and located at point P2-A (Fig. 2). Eighteen zircon crystals were chosen for analysis. These crystals were colorless, euhedral to subhedral, and elongated, some containing dark inclusions and/or microfractures. The isotopic results are presented in Table 4. Eight crystals presented a Pb signal too low to allow $^{207}Pb/^{206}Pb$ ratios to be measured or $^{206}Pb/^{204}Pb$ also too low ($^{206}Pb/^{204}Pb<2500$) to permit a reliable common lead correction. The remaining ten grains yielded ages between 2701±4 and 2748±3 Ma., with a mean value of 2732±6 Ma (MSWD=48; Fig. 9). Considering only the five crystals that provided older ages, a mean value of 2744±5 Ma (MSWD=4.9) is calculated (Fig. 9).

Pb–Pb in sulfides

As an attempt to determine the age of the mineralization and/or subsequent events that may have affected the ore bodies of the Visconde deposit, seven samples of chalcopyrite representing the main stage of mineralization were selected for Pb–Pb analysis. Three samples are from the sulfide-rich breccias and four from mono- or multi-mineral veins. The Pb isotopic results are shown in Table 5.

The analyses revealed the samples to be very radiogenic. For total digestion, the ranges of the $^{206}Pb/^{204}Pb$, $^{207}Pb/^{204}Pb$, and $^{208}Pb/^{204}Pb$ ratios are, respectively, 57.60–256.66, 24.90–61.92, and 56.17–270.98, while for leaching these ratios record values of 32.45 to 291.78, 18.21 to 66.00, and 46.26 to 87.81, respectively. On a $^{207}Pb/^{204}Pb$ vs. $^{206}Pb/^{204}Pb$ diagram, the samples submitted to total digestion yielded a linear array which corresponds to a calculated age of 2729±150 Ma with MSWD=3115 (Fig. 10a). A similar value (2736±100 Ma; MSWD=6131) was obtained using the whole dataset including total digestion and leaching (Fig. 10b).

Discussions

Evolution and sources of the hydrothermal fluids and metals

The types and stages of hydrothermal alteration at the Visconde deposit are similar to those commonly described for the IOCG deposit class (Hitzman et al. 1992; Williams et al. 2005) and reproduce fairly well what is observed in other Cu–Au deposits of Carajás, as Bacaba, Castanha, Alvo 118, Cristalino, and Sossego (Huhn et al. 1999; Villas et al. 2004; Monteiro et al. 2008; Moreto et al. 2011; Torresi et al. 2012).

Temperatures calculated using the oxygen isotope composition of different mineral pairs indicate that the Visconde hydrothermal system involved hot fluids (410 °C) at the earlier stages and cooler fluids (~240 °C) at the later stages. By the time chlorite precipitated overprinting the biotite-rich zones, the temperature was estimated at 285 °C based on the chlorite geothermometer (Craveiro 2011). In turn, the fluid inclusion data revealed a greater temperature range (>460 to ~160 °C) for the Visconde hydrothermal system, yet in a good agreement with the isotopic results. Concomitantly with the temperature drop, there was not only a decrease in fluid

Table 4 Pb isotopic ratios of zircon crystals from the Visconde granite. (c: corrected from common lead)

Zircon	*T* (°C)	Ratios	$^{204}Pb/^{206}Pb$	$(^{208}Pb/^{206}Pb)c$	2σ	$(^{207}Pb/^{206}Pb)c$	2σ	Step age	2σ
AR02/1	1500	20	34,483	0.16706	0.00133	0.19062	0.00038	2748	3
	1550	40	58,824	0.18825	0.00052	0.19057	0.00056	2747	5
AR02/3	1500	32	40,000	0.18134	0.00083	0.18805	0.00040	2726	4
	1550	34	47,619	0.18043	0.00042	0.19036	0.00032	2746	3
AR02/5	1500	22	34,483	0.18204	0.00173	0.18820	0.00068	2727	6
	1550	36	26,316	0.19710	0.00065	0.18793	0.00039	2725	3
AR02/6	1500	38	12,346	0.20137	0.00060	0.18532	0.00049	2701	4
AR02/7	1450	36	11,364	0.17523	0.00049	0.18906	0.00035	2734	3
	1500	26	10,000	0.17736	0.00194	0.18973	0.00086	2740	7
AR02/9	1500	32	24,390	0.18142	0.00075	0.18921	0.00028	2736	2
AR02/13	1450	12	4348	0.17060	0.00142	0.18715	0.00100	2718	9
	1450	30	6289	0.19617	0.00550	0.18734	0.00023	2719	2
AR02/14	1500	34	19,608	0.15891	0.00156	0.18839	0.00064	2729	6
	1550	14	10,638	0.15657	0.00116	0.18977	0.00043	2741	4
AR02/15	1500	8	18,519	0.17165	0.00049	0.18786	0.00065	2724	6
	1550	32	58,824	0.17698	0.00059	0.18972	0.00030	2740	3
AR02/18	1500	40	10,309	0.19798	0.00190	0.18834	0.00107	2728	9

salinity (from 56 to 7 wt.% equiv. NaCl) but also a progressive ^{18}O depletion in the fluid (+9.4 to −1.3‰; Fig. 11).

During the early sodic-calcic alteration, $\delta^{18}O_{H_2O}$ values were higher (+3.3 to +9.4‰ at 410°–355 °C). Magnetite, in particular, precipitated from a fluid with a more restricted range of $\delta^{18}O_{H_2O}$ (+5.6 to +7.4‰ at 410 °C). In the potassic stage, coincident with the development of local ductile shear zones, the $\delta^{18}O_{H_2O}$ values were slightly lower than those of the previous stages (+4.8 to +7.2‰ at 355 °C). All these $\delta^{18}O_{H_2O}$ ranges are consistent with fluids derived from magmatic sources (Taylor 1997), especially those responsible for the early alteration types.

The later stages (sodic-calcic and calcic-magnesian alterations), typically formed in veins outside the mineralized breccias, are related to fluids with temperatures of 230 °C and $\delta^{18}O_{H_2O}$ values between −1.3 and +4.4‰, suggesting the involvement of surficial water. This hypothesis is corroborated by the fluid inclusion data that show lower salinity for the fluid that had circulated through the deposit rocks at the later stages. The salinity decreased from ~30 to 7 wt.% equiv. NaCl, indicating dilution, although at a constant temperature around 160–200 °C (Fig. 12).

The $\delta^{18}O_{H_2O}$ and δD_{H_2O} values for fluids related to the early sodic-calcic and potassic alteration zones plot in the metamorphic water field, close to the magmatic field. Some actinolite values are compatible with magmatic waters, whereas chlorite and epidote, corresponding to the later alteration zones, tend to approach the meteoric water line (Fig. 13).

A metamorphic signature is plausible because a regional metamorphic event lasting from 2.76 to 2.73 Ga (Machado et al. 1991; Pinheiro and Holdsworth 2000) is recorded in both the Transition and Carajás domains. This event is related to the inversion of the Carajás basin where the metamorphic conditions range from the lower greenschist to upper amphibolite facies. According to Taylor (1974, 1997), dehydration water is the dominant constituent of metamorphic pore fluids only at high grades, whereas formation waters prevail at lower grades. Some samples from the Visconde deposit plot where the metamorphic and formation water fields overlap (Fig. 13). Formation water could have migrated toward the Visconde deposit area from the nearby Carajás basin, particularly from

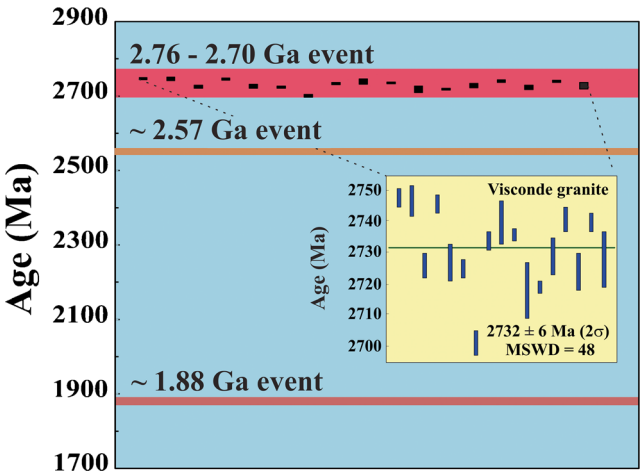

Fig. 9 Single zircon Pb-evaporation age diagram for the Visconde granite showing the main Neoarchean and Paleoproterozoic episodes of granitogenesis in the CMP (*deep pink* and *brown lines*). The *enclosed light yellow diagram* displays the age spectrum using all data presented in Table 1. The *vertical bars* represent the errors for each zircon grain, and the *horizontal green line* corresponds to the weighted average crystallization age

Table 5 Pb isotope ratios chalcopyrite samples from the Visconde deposit (2σ=analytical error)

Sample	$^{206}Pb/^{204}Pb$	2σ	$^{207}Pb/^{204}Pb$	2σ	$^{208}Pb/^{204}Pb$	2σ
Leaching						
12-37 L1	55.27	0.13	22.33	0.06	46.26	0.11
12-37 L2	79.82	0.52	28.06	0.18	56.72	0.38
12-37 L3	65.20	0.75	24.92	0.28	58.22	0.66
12-37 L4	75.37	0.99	27.63	0.35	60.80	0.77
12-37 L5	105.40	0.12	36.29	0.04	69.32	0.08
12-37 L6	43.04	0.52	21.33	0.29	47.71	0.58
F36-28a L1	172.81	1.25	42.61	0.31	60.18	0.43
F36-28a L2	291.78	1.25	66.00	0.28	87.81	0.37
F36-28a L3	105.10	4.19	30.82	1.22	55.84	2.25
F36-28a L4	93.99	6.29	27.95	1.93	49.53	3.45
F36-28a L5	142.84	0.49	44.17	0.15	55.64	0.18
F36-28a L6	78.14	0.64	28.74	0.23	50.07	0.41
F36-28b L1	111.35	6.33	30.652	1.74	49.14	2.82
F36-28b L2	138.54	0.251	43.69	0.09	54.73	0.12
F36-28b L3	138.92	5.724	39.32	1.70	59.41	2.59
F36-28b L4	144.94	0.156	44.63	0.07	56.05	0.12
F36-28b L5	177.09	1.361	45.51	0.36	65.94	0.53
F36-28b L6	278.87	4.795	63.46	1.06	82.98	1.43
10-50 L1	32.48	0.24	18.21	0.14	47.17	0.37
10-50 L2	41.41	0.18	20.67	0.08	53.69	0.22
10-50 L3	44.99	0.72	21.16	0.38	55.14	0.99
10-50 L4	46.60	0.22	21.83	0.10	57.42	0.26
10-50 L5	56.76	0.33	23.63	0.18	60.82	0.46
10-50 L6	61.02	0.13	25.36	0.07	65.57	0.18
Total digestion						
10-50 D	57.60	0.12	24.90	0.06	64.81	0.19
5-32 D	85.70	0.02	29.39	0.01	89.15	0.04
12-37 D	89.51	0.76	32.36	0.26	64.56	0.57
F36-28 D	122.65	0.48	38.48	0.15	119.22	0.50
F36-171 D	137.53	0.18	41.07	0.06	56.17	0.08
F36-25 D	184.12	0.39	50.35	0.12	112.83	0.27
14-37 D	256.69	1.32	61.92	0.33	270.95	1.55

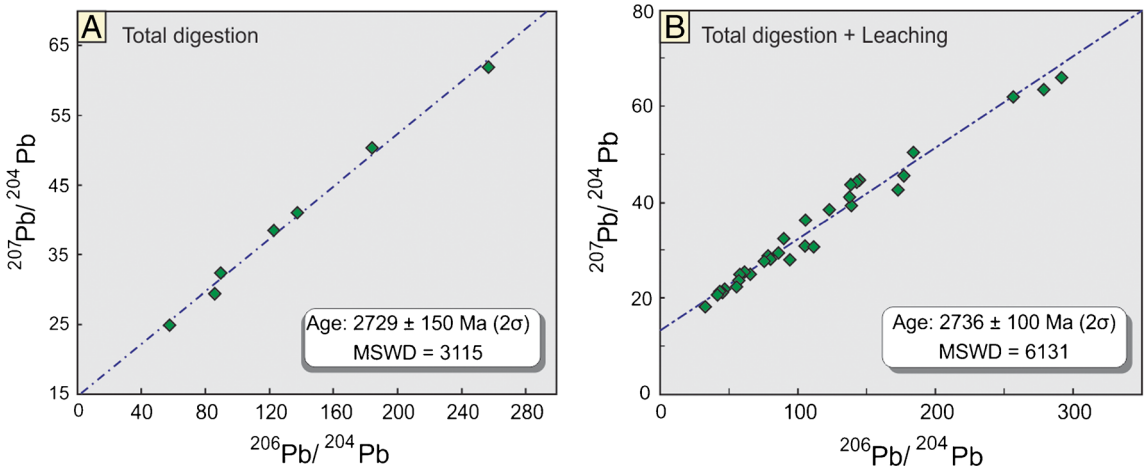

Fig. 10 $^{207}Pb/^{204}Pb$ vs. $^{206}Pb/^{204}Pb$ diagrams for chalcopyrite from the Visconde deposit. **a** Total digestion. **b** All data (digestion and leaching). Analytical error=2σ

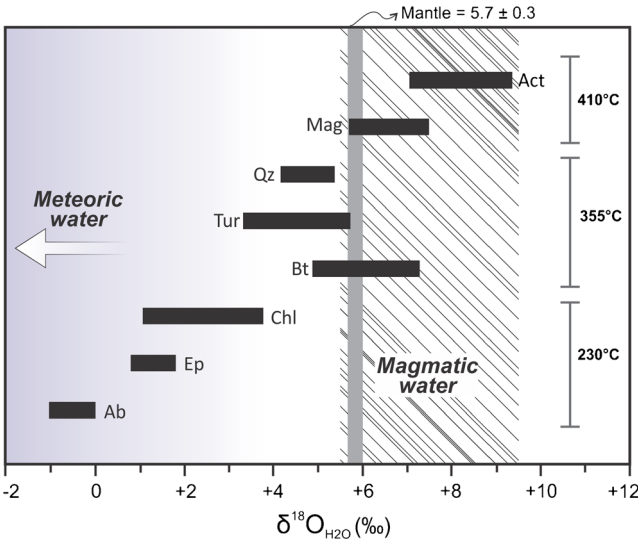

Fig. 11 Range of oxygen isotope composition of the fluids (*black bars*) that caused alteration and mineralization in the Visconde deposit. The *vertical lines on the right* represent the temperatures used in the calculations for a given set of minerals. The magmatic and meteoric water fields are from Taylor (1997). *Ab* albite, *Act* actinolite, *Bt* biotite, *Chl* chlorite, *Ep* epidote, *Mag* magnetite, *Qz* quartz, *Tur* tourmaline

rocks submitted to less- intense regional metamorphism. Along its pathway, this water interacted with the deposit metamorphic host rocks and its composition was progressively modified. As a result, it acquired a metamorphic isotopic character at the same time that it mixed with pre-existing metamorphic fluids.

Given that the dehydration water generally presents low salinity, the involvement of formation water is also an attractive hypothesis to explain the high salinities (up to 56 wt.% equiv. NaCl) recorded in the Visconde hydrothermal fluids. Waters trapped within the sediment interstices tend to have their salinity increased and to undergo compositional changes during the residence time (Taylor 1997), becoming a potential reservoir for metals and ligands. That hypothesis gains further support from B isotopic data and Cl/Br and Na/Cl ratios, which have indicated the interaction of fluids with evaporite beds in other Carajás IOCG deposits (Xavier et al. 2008, 2010).

A few actinolite and biotite samples from early alteration stage yielded δD_{H_2O} values characteristic of water dissolved in felsic magmas that did not undergo boiling (Taylor 1992). These values may indicate the involvement of magmatic fluids in the Visconde hydrothermal system, especially in the early stages, despite the overlapping with metamorphic fluids. Several authors suggested a magmatic origin for the IOCG mineralizing fluids (e.g., Pollard 2001; Groves et al. 2010).

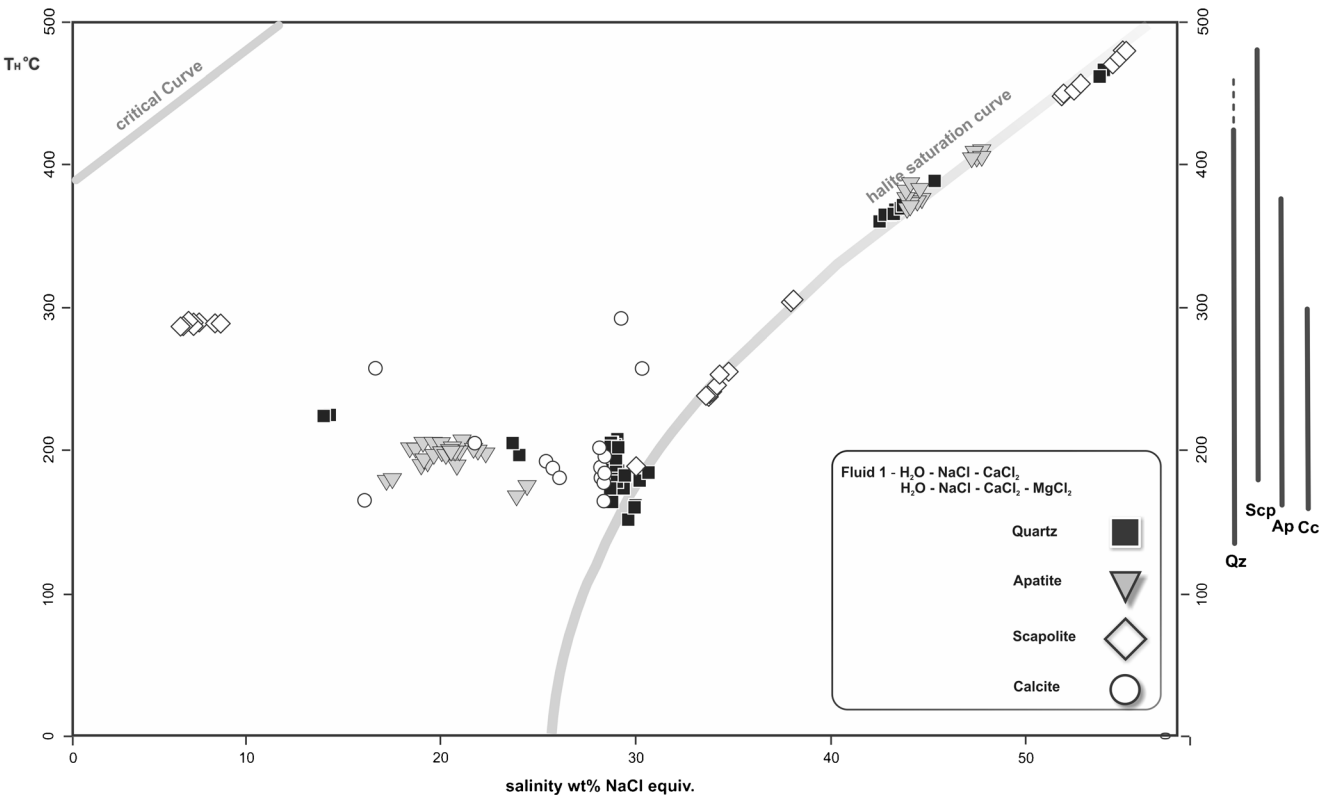

Fig. 12 Salinity vs homogenization temperature diagram depicting two important dilution trends for fluid 1, one with a high-temperature drop (460 to 160–200 °C) and the other without significant temperature change. The *vertical bars* represent the temperature ranges of formation of quartz (*Qz*), scapolite (*Scp*), apatite (*Ap*), and calcite (*Cc*). The halite saturation curve and critical curve are from Bodnar et al. (1989) and Knight and Bodnar (1989), respectively

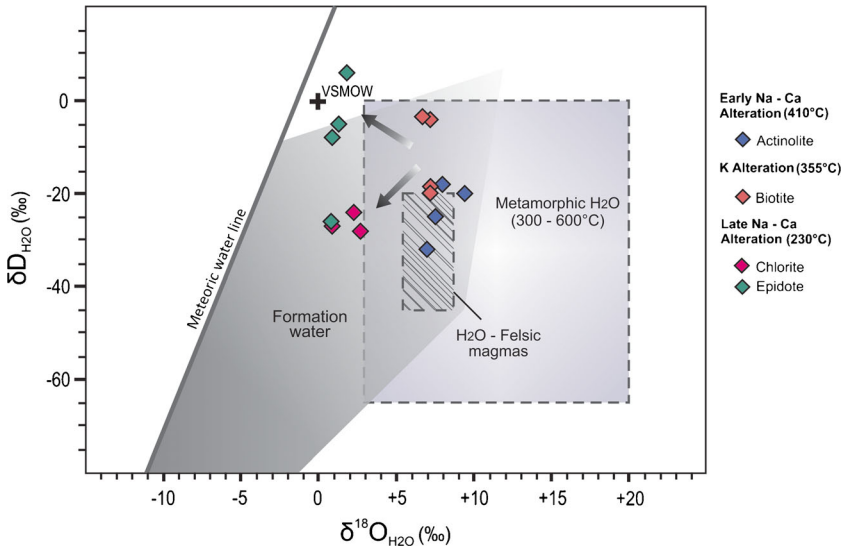

Fig. 13 Oxygen and hydrogen isotope composition of fluids responsible for the alteration and mineralization in the Visconde deposit. Next to each alteration type (*in parentheses*) are the temperatures used in the calculations. Metamorphic, magmatic, and formation water fields are from Sheppard (1986), Taylor (1992), and Taylor (1997), respectively

For the Visconde deposit, this is a permissive hypothesis because there is obvious spatial relationship between ore and intrusive bodies of the Planalto suite granites and gabbros/diorites. Mixing of metamorphic with magmatic fluids would then be a reasonable interpretation and, in this case, those intrusive rocks could be most likely magmatic sources.

Assuming the hypothesis of mixing, the fluid composition changed from the sodic-calcic (actinolite) to the potassic (biotite) stage, moving away from the magmatic field due to the greater contribution of metamorphic water to the solutions that precipitated that mica. This mixing resulted in a steep decrease in both temperature (460 to 230 °C) and salinity (58 to 35 wt.% equiv. NaCl) of the fluid responsible for these types of hydrothermal alteration (Fig. 11). From biotitization to chloritization, the $\delta^{18}O_{H_2O}$ and δD_{H_2O} values varied significantly with the progressive depletion in ^{18}O and D, indicating now mixing with meteoric waters (Fig. 10). In turn, most epidote samples present δD_{H_2O} values fairly distinct and tend to approach that of seawater (Fig. 13). A similar trend has been found in the neighboring Sossego deposit (Monteiro et al. 2008). However, Dilles et al. (1992) claim that the epidote δD_{H_2O} data should be interpreted with caution, since this mineral is extremely susceptible to D fractionation. The later alteration stages seem to have been dominated by surficial water, whose influx was largely favored by the brittle regime that then prevailed. Because the mineralization was contemporaneous with the later hydrothermal stages, dilution and decreasing temperature were the main factors causing abundant sulfide precipitation.

All $\delta^{34}S$ values of the Visconde chalcopyrite, but a single datum are positive and deviate very slightly from the composition of magmatic sulfur. The narrow $\delta^{34}S$ range ($-1.2 \leq \delta^{34}S \leq +3.4$ ‰) allows inferring that sulfur did not undergo any significant degree of isotopic fractionation while being transported by the hydrothermal fluid. Most likely, the fluid was reducing otherwise a larger fractionation and a greater spread of $\delta^{34}S$ values would be expected (Rye and Ohmoto 1974). The abundant precipitation of magnetite prior to the main sulfide mineralization certainly consumed a large amount of oxygen causing a decrease of the oxidation potential. The oxygen fugacity of the fluid dropped to levels that hindered the co-precipitation of the oxide and sulfide phases during the main ore formation. Under these reducing conditions, the range of δ^{34}S values of the sulfide may be assumed to represent closely that of the fluid from which it precipitated (Ohmoto and Goldhaber 1997). After the main mineralization event, the O_2 fugacity increased as supported by the local occurrence of late gypsum and hematite-bearing veins.

Sulfide precipitation occurred during all alteration stages, but it was more significant after the intense biotitization of the rocks and was contemporaneous with the calcic-magnesian alteration. Thus, fluids transported S species from the very beginning of the Visconde's hydrothermal history. The Visconde sulfur isotope composition is partly consistent with the mantle source ($\delta^{34}S = 0 \pm 1$‰; Eldridge et al. 1991) and compatible with the interval commonly attributed to sulfur from magmatic reservoirs ($\delta^{34}S = 0 \pm 5$‰; Ohmoto and Goldhaber 1997). Those species most likely were leached from magmatic sulfides present in the metavolcanic rocks from the Carajás basin or ultramafic rocks and granitic intrusions from the Transition domain, or both. On the other hand, the less oxidizing conditions of the Archean atmosphere may not have precluded the extraction of some sulfur from evaporitic sequences. The $\delta^{34}SSO4^{2-}$ values in these reservoirs vary from ≈2 to 5‰ between ≈3.5 and ≈2.7 Ga (Ohmoto and Goldhaber 1997), being compatible with the S isotope composition of the Visconde deposit.

Compared with other Cu–Au Carajás deposits (Fig. 14), the Visconde sulfide $\delta^{34}S_{VCDT}$ values are similar to those from the Cristalino, Pista, Bacaba, Castanha, Jatobá, and Salobo

deposits (Fig. 13). In general, heavier S isotopic compositions have been found in the Sossego ore bodies (Sequeirinho, Sossego, Baiano, and Curral) and Alvo 118, for which the incorporation of ^{34}S from surficial sources during the sulfide precipitation is a viable hypothesis (Torresi et al. 2012).

Ages of the Visconde granite and mineralizing event

The set of Pb–Pb data obtained on zircon from the Visconde granite does not allow determining an accurate and reliable age for its emplacement. The high MSWD value (48) of the age (2732±6 Ma) obtained on the whole population of analyzed zircons reveals a complex U–Pb behavior and may reflect the effects of postcrystallization radiogenic lead loss by metamictization. The existence of slightly older inherited cores cannot be ruled out and may also account for the scattering of the results.

Even poorly constrained, the Pb–Pb results allow discarding a Paleoproterozoic age for this granite. The 2748–2704 Ma range obtained for the zircons of the Visconde granite is similar to those of other granites emplaced into the rocks of both the Transition and Carajás domains, such as the Serra do Rabo intrusion and the Planalto suite (Fig. 9). Pb–Pb zircon dating of several intrusions that have been correlated to the Planalto Suite yielded ages from 2747± 2 Ma (Huhn et al. 1999) to ~2730 Ma (Sardinha et al. 2004; Feio et al. 2012). A similar U–Pb zircon age of 2743±1.6 Ma was also determined for the Serra do Rabo granite (Sardinha et al. 2006). Although mapped as a different stratigraphic unit, this intrusion mineralogically and texturally resembles the Planalto suite stocks. Recently, younger ages (2729±17, 2710±10, and 2706±5 Ma) have been obtained for zircon grains from Planalto granites using the U–Pb LA-ICP-MS technique (Feio et al. 2012). The fact that the zircon ages of the Visconde granite lie within the range of ages attributed to the crystallization of the Planalto suite suggests that it belongs to this suite, in agreement with what was previously proposed on the basis of petrographic features (Feio et al. 2012; Craveiro et al. 2012).

Pb–Pb dating of the Visconde ore yielded ages of 2.73± 0.15 and 2.74±0.10 Ga (Fig. 10a, b), which, despite the large errors, are coherent with the geology of the area and similar to the Archean age of the main Carajás Cu–Au mineralization. Similar ages have been obtained for the Cristalino deposit (2716±36 Ma, Pb–Pb in pyrite, Soares et al. 2001) and for the Sequeirinho ore body of the Sossego mine (2712±4.7 Ma, U–Pb in monazite, Moreto et al. 2013). These ages indicate a Neoarchean mineralization event, but they should be evaluated in the light of other geological events recorded in the Transition domain.

In IOCG provinces, it is of particular interest to assess the genetic relationship between mineralization and magmatic activity (e.g., Candelaria in Chile, Olympic Dam in Australia; Mathur et al. 2002; Bastrakov et al. 2007). For the Carajás Cu–Au deposits, available geochronological data, based on Pb–Pb, U–Pb, and Re–Os systematics, have indicated three main mineralization ages, coincident with regional magmatic events that occurred at 2.76–2.70, ca.2.57, and 1.88 Ga. The first refers to the formation of the Estrela Granitic complex, Planalto suite, Plaquê suite, and correlated granites (Soares et al. 2001; Galarza et al. 2008); the second event is represented by the Old Salobo and Itacaiunas granitic stocks (Requia et al. 2003; Tallarico et al. 2005); and the third is represented by the Paleoproterozoic A-type granitic plutonism (Tallarico 2003; Neves et al. 2006; Moreto et al. 2013).

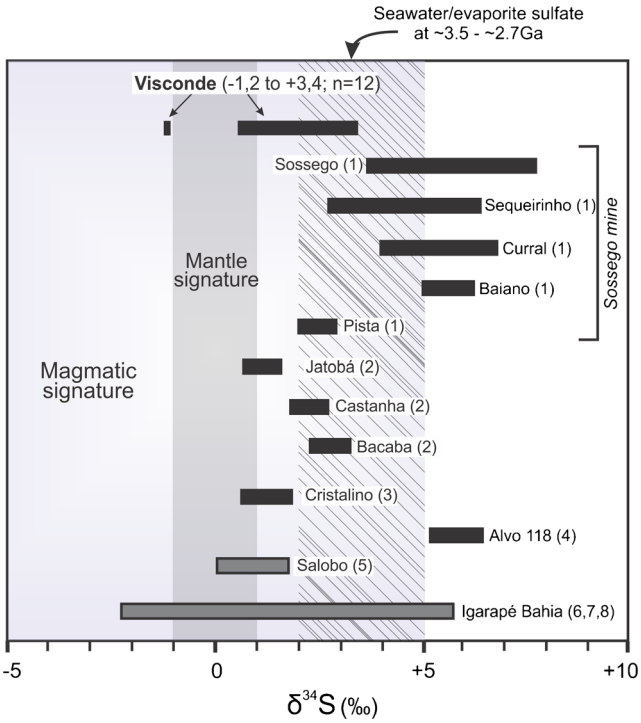

Fig. 14 Sulfur isotope composition of sulfides from the Visconde deposit compared with other Cu–Au Carajás deposits. *1*, Monteiro et al. (2008); *2*, Monteiro et al. (2007); *3*, Ribeiro et al. (2009); *4*, Torresi et al. (2011); *5*, Requia and Fontboté (2001); *6*, Tazava and Oliveira (2000); *7*, Villas et al. (2001); *8*, Dreher et al. (2008). Magmatic field and Archean sulfate (*crosshatched*) are from Ohmoto and Goldhaber (1997); mantle signature is from Eldridge et al. (1991)

The time interval in which the Planalto suite formed not only includes the age of the mineralization obtained here but also marks a tectonically active period in the Carajás Province. Similarly to the Sossego deposit (Villas et al. 2005; Monteiro et al. 2008), the altered zones in the Visconde deposit display textures indicative that the hydrothermal system developed under a ductile to brittle structural regime. Hence, it is possible that both the emplacement of the Planalto granitic rocks and the Visconde hydrothermal alteration took place during the same tectonic episode. The occurrence of the 1.88 Ga Rio Branco granite (Santos et al. 2013a, b) at approximately 15 km from the Visconde deposit does not a priori rule out a genetic

link with the Paleoproterozoic A-type granites. However, in contrast to what was observed for the Sossego and Alvo 118 deposits (Tallarico 2003; Neves et al. 2006; Moreto et al. 2013), no isotopic evidence has been detected indicating that the Visconde Pb–Pb system was affected at that time, and the influence of a Paleoproterozoic event is unlikely.

Conclusions

The Visconde deposit is hosted mainly by metadacites, the Serra Dourada granite, and gabbros/diorites of Meso- and Neoarchean age. The more conspicuous ore bodies occur as breccias supported by a matrix dominantly composed of chalcopyrite. The mineral associations give a Cu–Au-Fe–Ni–ETRL–B–P signature to the ore.

In the outer portions of the ore bodies, hydrothermal alteration zones are well developed. The earlier and more pervasive sodic and sodic-calcic types were controlled by regional shear zones and almost completely changed the primary mineralogy of the rocks. Isotope data of silicate minerals from these alteration zones reveal hot (410 to 355 °C) and ^{18}O-rich ($\delta^{18}O_{H_2O}$ =+4.2 to +9.4‰) fluids dominantly formed by metamorphic waters, most likely derived from the Carajás basin rocks. Fluid inclusion data indicate that the hydrothermal fluids responsible for these alteration zones were very saline (up to 58 wt.% equiv. NaCl) and may have reached temperatures above 460 °C. Some contribution from magmatic sources is permissive, in which case the Planalto suite is assumed to be the most viable source.

Considering that the Itacaiúnas Supergroup units do not host the Visconde deposit, large-scale structures would have enabled migration of the fluids from the basin to the basement. Fluids with similar oxygen isotope composition ($\delta^{18}O_{H_2O}$ =+4.8 to +7.2‰ at 356 °C) promoted severe biotitization of the rocks (potassic alteration) that was controlled by local shear zones, as evidenced by the development of mylonitic foliation at different scales. The fluids experienced not only a significant temperature drop, but also a dilution process during which fluid salinity decreased to 30 wt.% equiv. NaCl approximately.

Major precipitation of chalcopyrite (±bornite±chalcocite± digenite) occurred later during the brittle regime to which the rocks had been subjected. These sulfides occur mainly in veins and breccias associated with calcic-magnesian minerals, whose isotopic oxygen signature suggests the involvement of connate and meteoric fluids ($\delta^{18}O_{H_2O}$ =−1.3 to +3.7‰) at lower temperatures (230±11 °C). As a result, the fluids became progressively less saline (from 30 to 7 wt.% equiv. NaCl) and colder, with temperatures as low as ~160 °C. Thus, dilution and temperature decrease were most likely the main mechanisms that triggered the precipitation of large amounts of sulfides. The sulfur isotope composition ($\delta^{34}S_{VCDT}$=−1.2 to 3.4‰) indicates relatively reducing conditions for the fluid, which had much of its oxygen consumed by the earlier precipitation of abundant magnetite. This signature is compatible with a magmatic source for sulfur, which could have been either exsolved during the crystallization of a granitic magma or leached from sulfides originally present in pre-existing igneous rocks. Basement Mesoarchean ultramafic, felsic volcanic and granitic rocks could have also supplied components to the hydrothermal system, as the Pb data suggest.

Pb–Pb ages for the Cu–Au mineralization are imprecise (2.73±0.15 Ga and 2.74±0.10 Ga). Nevertheless, they indicate a Neoarchean age for the formation of the Visconde main ore bodies. Despite the large errors, these ages are consistent with the geology of the area and with the 2.75 Ga IOCG mineralizing event that has been recorded in Carajás.

Textural evidence shows that the hydrothermal system was conditioned by a structural regime that evolved from ductile to brittle, which may be indicative of its contemporaneity with the transpressive tectono-thermal event that occurred in the Transition domain during the Neoarchean. Although the geochronological data do not define more precisely the age of the Visconde mineralization, it is very unlikely that it was temporally related to the 2.5 or 1.88 Ga magmatic events, related the formation of other Carajás Cu–Au deposits (Tallarico 2003; Requia et al. 2003; Tallarico et al. 2005; Neves et al. 2006; Moreto et al. 2013).

The types and sequence of the alteration stages, structural controls, association with regional magmatism, style of mineralization, and Fe–Cu–Au metallic signature allow including the Visconde deposit in the IOCG class, similarly to other Cu–Au deposits of the Transition domain.

Acknowledgments Thanks are extended to the National Council for Science and Technological Development (CNPq), which granted A.R.C.S. a scholarship during her graduate studies at the Federal University of Pará (UFPA). This research was funded by the Geosciences Institute of Amazon-Geociam (INCT program–CNPq/MCT/FAPESPA 573733/2008-2). We are grateful to the VALE Mining Company for permitting access to the Visconde deposit and assigning borehole samples and some internal information, particularly to geologist Benevides Aires for his assistance in the field. Dr. Claudio Lamarão (MEVUFPA), Dr. Alcides Sial (LABISE-UFPE), and the technical staff of both PARA-ISO and LABISE laboratories are thanked for their invaluable support during the sample analyses. Thanks are also due to two anonymous reviewers and to the Associate Editor David Craw for their constructive criticism and insightful suggestions, which greatly improved this paper.

References

Augusto RA, Monteiro LVS, Xavier RP, Souza Filho CR (2008) Zonas de alteração hidrotermal e paragênese do minério de cobre do Alvo Bacaba, Província Mineral de Carajás (PA). Rev Brasil Geocienc 38: 263–277

Avelar VG, Lafon JM, Correia FC Jr, Macambira EMB (1999) O Magmatismo arqueano da região de Tucumã-Província Mineral de Carajás: novos resultados geocronológicos. Rev Brasil Geocienc 29: 454–460

Barreto CJS, Lafon JM, Rosa Costa LT, Dantas EL (2013) Paleoproterozoic granitoids from the northern limit of the Archean Amapá block (Brazil), Southeastern Guyana Shield: Pb–Pb evaporation in zircons and Sm–Nd geochronology. J South Am Earth Sci 45:97–116

Barros CEM, Barbey P, Boullier AM (2001) Role of magma pressure, tectonic stress and crystallization progress in the emplacement of syn-tectonic granites. The A-type Estrela Granite Complex (Carajás Mineral Province, Brazil). Tectonophysics 343:93–109

Bastrakov EN, Skirrow RG, Davidson GJ (2007) Fluid evolution and origins of iron oxide Cu–Au prospects in the Olympic Dam District, Gawler Craton, South Australia. Econ Geol 102:1415–1440

Bodnar RJ (1993) Revised equation and table for determining the freezing point depression of H_2O–NaCl solutions. Geochim Cosmochim Acta 57:683–684

Bodnar RJ, Sterner SM, Hall DL (1989) SALTY: a FORTRAN program to calculate compositions of fluid inclusions in the system NaCl–KCl–H_2O. Comput Geosci 15:19–41

Borisenko NF (1977) Study of the salt composition of solutions in gas–liquid inclusions in minerals by the cryometric method. Sov Geol Geophys 18:11–19

Botelho NF, Moura MA, Teixeira LM, Olivo GR, Cunha LM, Santana UM (2005) Caracterização geológica e metalogenética do depósito de Cu ± (Au, W, Mo, Sn) Breves, Carajás. In: Marini OJ, Queiroz ET, Ramos BW (ed) Caracterização de depósitos minerais em distritos minerais da Amazônia. DNPM-FINEP-ADIMB, pp 335–390

Bottinga Y, Javoy M (1973) Comments on oxygen isotope geothermometry. Earth Planet Sci Lett 20:250–265

Carvalho ER (2009) Caracterização geológica e gênese das mineralizações de óxido de Fe−Cu−Au e metais associados na Província Mineral de Carajás: estudo de caso do depósito de Sossego. Ph.D. thesis, Universidade Estadual de Campinas, 151 p

Chiaradia M, Banks D, Cliff R, Maschik R, Haller A (2006) Origin of fluids in iron oxide–copper–gold deposits: constraints from $\delta^{37}Cl$, $^{87}Sr/^{86}Sri$ and Cl/Br. Miner Deposita 41:565–573

Clayton R, Mayeda TK (1963) The use of bromine pentafluoride in the extraction of oxygen from oxides and silicates for isotopic analysis. Geochim Cosmochim Acta 27:43–52

Companhia Vale do Rio Doce-VALE (2003) Programa Polo Sossego, Alvo Visconde, mapa geológico. Escala gráfica

Craveiro GS (2011) Geologia, fluidos hidrotermais e origem do depósito cupro-aurífero Visconde, Província Mineral de Carajás. MSc dissertation, Universidade Federal do Pará, 151 p

Craveiro GS, Villas RNN, Silva ARC (2012) Depósito Cu–Au Visconde, Carajás (PA): geologia e alteração hidrotermal das rochas encaixantes. Rev Brasil Geocienc 42:453–470

Dall'Agnol R, Teixeira NP, Rämö OT, Moura CAV, Macambira MJB, Oliveira DCO (2005) Petrogenesis of the Paleoproterozoic Rapakivi A-type granite of the Archean Carajás Metallogenetic Province, Brazil. Lithos 80:101–129

Dall'Agnol R, Oliveira MA, Almeida JAC, Althoff FJ, Leite AAS, Oliveira DC, Barros CEM (2006) Archean and paleoproterozoic granitoids of the Carajás Metallogenic Province, eastern Amazonian Craton. In: Symposium on Magmatism, Crustal Evolution, and Metallogenesis of the Amazonian Craton, Field trips guide, pp 99–150

Davis WD, Lowenstein TK, Spencer RJ (1990) Melting behavior of inclusions fluids in laboratory grown halite crystals in the systems NaCl–H_2O, NaCl–KCl–H_2O, NaCl–$MgCl_2$–H_2O and NaCl–$CaCl_2$–H_2O. Geochim Cosmochim Acta 54:591–601

Dias GS, Macambira MJB, Dall'Agnol R, Soares ADV, Barros CEM (1996) Datação de zircões de sill de metagabbro: comprovação da idade arqueana da Formação Águas Claras, Carajás-Pará. In: V Simpósio de Geologia da Amazônia, Belém, Extended Abstracts, pp 376–379

Dilles JH, Solomon GC, Taylor HP Jr, Einaudi MT (1992) Oxygen and hydrogen isotope characteristics of hydrothermal alteration at the Ann-Mason porphyry copper deposit, Yerington, Nevada. Econ Geol 87:44–63

Docegeo - Rio Doce Geologia e Mineração S.A (1988) Revisão litoestratigráfica da Província Mineral de Carajás. In: Proceedings, Congr Bras Geol, Belém, 1:11–54

Dreher AM, Xavier RP, Taylor BE, Martini S (2008) New geologic, fluid inclusion and stable isotope studies on the controversial Igarapé Bahia Cu–Au deposit, Carajás Province, Brazil. Miner Deposita 43:162–184

Eldridge CS, Compston W, Williams IS, Harris JW, Bristow JW (1991) Isotope evidence for the involvement of recycled sediments in diamond formation. Nature 353:649–653

Feio GRL, Dall'Agnol R, Dantas EL, Macambira MJB, Gomes ACB, Sardinha AS, Oliveira DC, Santos RD, Santos PA (2012) Geochemistry, geochronology, and origin of the Neoarchean Planalto Granite suite, Carajás, Amazonian craton: a-type or hydrated charnockitic granites? Lithos 151:57–73

Feio GRL, Dall'Agnol R, Dantas EL, Macambira MJB, Santos JOS, Althoff FJ, Soares JEB (2013) Archean granitoid magmatism in the Canaã dos Carajás area: implications for crustal evolution of the Carajás province, Amazonian craton, Brazil. Precambrian Res 227:157–185

Galarza MA, Macambira MJB, Villas RN (2008) Dating and isotopic characteristics (Pb and S) of the Fe oxide–Cu–Au–U–REE Igarapé Bahia ore deposit, Carajás Mineral Province, Pará state, Brazil. J South Am Earth Sci 25:377–397

Gibbs AK, Wirth KR, Hirata WK, Olszewski JWJ (1986) Age and composition of the Grão Pará Group volcanics, Serra dos Carajás. Rev Brasil Geocienc 16:201–211

Gomes ACB, Dall'Agnol R (2007) Nova associação tonalítica-trondhjemítica neoarqueana na região de Canaã dos Carajás: TTG com altos conteúdos de Ti, Zr e Y. Rev Brasil Geocienc 37:182–193

Graham CM, Sheppard SMF, Heaton THE (1980) Experimental hydrogen isotope studies: I. Systematics of hydrogen isotope fractionation in the systems epidote-H_2O, zoisite-H_2O and AlO(OH)-H_2O. Geochim Cosmochim Acta 44:353–364

Graham CM, Harmon RS, Sheppard SMF (1984) Experimental hydrogen isotope studies: hydrogen isotope exchenge between amphibole and water. Am Mineral 69:128–138

Grainger CJ, Groves DI, Tallarico FHB, Fletcher IR (2008) Metalligenesis of the Carajás Mineral Province, Southern Amazon Craton, Brazil: varying styles of Archean through Paleoproterozoic to Neoproterozoic base- and precious-metal mineralization. Ore Geol Rev 33:451–489

Groves DI, Bierlein FP, Meinert LD, Hitzman MW (2010) Iron oxide copper–gold (IOCG) deposits through Earth history: implications for origin, lithospheric setting, and distinction from other epigenetic iron oxide deposits. Econ Geol 105:641–654

Hitzman MW, Oreskes N, Einaudi MT (1992) Geological characteristics and tectonic setting of Proterozoic iron oxide (Cu–U–Au–REE) deposits. Precambrian Res 58:241–287

Huhn SRB, Macambira MJB, Dall'Agnol R (1999) Geologia e geocronologia Pb/Pb do granito alcalino Arqueano Planalto, Região da Serra do Rabo, Carajás-PA. In: VI Simpósio de Geologia da Amazônia, pp 463–466

Klötzli US (1997) Single zircon evaporation thermal ionisation mass spectrometry: method and procedures. Analyst 122: 1239–1248

Knight CL, Bodnar RJ (1989) Synthetic fluid inclusions: IX. Critical PVTX properties of NaCl–H_2O solutions. Geochim Cosmochim Acta 53:3–8

Kober B (1986) Whole-grain evaporation for $^{207}Pb/^{206}Pb$-age investigations on single zircons using a double-filament thermal ion source. Contrib Mineral Petrol 93:482–490

Kober B (1987) Single grain evaporation combined with Pb emitter bedding $^{207}Pb/^{206}Pb$ investigations using thermal ion mass spectrometry and implications to zirconology. Contrib Mineral Petrol 96: 63–71

Kyser TK, Kerrich R (1991) Retrograde exchange of hydrogen isotopes between hydrous minerals and water at low temperatures. Geochem Soc Spec Publ 3:409–422

Lafon JM, Macambira MJB, Pidgeon RT (2000) Zircon U–Pb SHRIMP dating of Neoarchean magmatism in the southwestern part of the Carajás Province (eastern Amazonian Craton, Brazil). In: Intern Geol Congr, Abstracts, CD-ROM

Lindenmayer ZG (1990) Salobo Sequence, Carajás, Brazil: geology, geochemistry and metamorphism. Ph.D. thesis, London, Canada, University of Western Ontario, 407 p

Lindenmayer ZG, Pimentel MM, Ronchi LH, Althoff FJ, Laux JH, Fleck A, Baecker CA, Carvalho DB, Nowatzki AC (2005) Geologia do depósito de Cu–Au de Gameleira, Serra dos Carajás, Pará. In: Marini OJ, Queiroz ET, Ramos BW (eds) DNPM/ADIMB—Caracterização de depósitos auríferos em distritos mineiros brasileiros, Brasília, pp 80–139

Ludwig K (2008) Isoplot 3.6: Berkeley Geochronology Center Special Publication 4, 77p

Macambira EMB, Tassinari CCG (1998) Estudos Sm/Nd no complexo máfico-ultramáfico da Serra da Onça-sul do Pará: implicações geocronológicas e geotectônicas. In: Proceedings, Congr Bras Geol, p 463

Macambira BEM, João XSJ, Souza EC (1996) Geolgical and petrochemical aspects of the Plaquê granite–Southern of the Pará Satate. In: Symposium on Archean terranes of the South American plataform, Extended Abstracts, pp 73–75

Machado N, Lindenmayer Z, Krogh TH, Lindenmayer ZG (1991) U–Pb geochronology of Archaean magmatism and basement reactivation in the Carajás area, Amazon shield, Brazil. Precambrian Res 49: 329–354

Mathur R, Marschik R, Ruiz J, Munizaga F, Leveille RA, Martin W (2002) Age of mineralization of the Candelaria Fe oxide–Cu–Au deposit and the origin of the Chilean Iron Belt, based on Re–Os isotopes. Econ Geol 97:59–71

Matsuhisa Y, Goldsmith JR, Clayton RN (1979) Oxygen isotopic fractionation in the system quartz-albite-anorthite-water. Geochim Cosmochim Acta 43:1131–1140

Monteiro LVS, Xavier RP, Souza Filho CR, Augusto RA (2007) Aplicação de isótopos estáveis ao estudo dos padrões de distribuição das zonas de alteração hidrotermal associados ao sistema de óxido de ferro-cobre-ouro Sossego, Província Mineral de Carajás. In: Cong Bras Geoq, Abstracts, CD-ROM

Monteiro LVS, Xavier RP, Carvalho ER, Hitzman MW, Johnson AC, Souza Filho CR, Torresi I (2008) Spatial and temporal zoning of hydrothermal alteration and mineralization in the Sossego iron oxide–copper–gold deposit, Carajás Mineral Province, Brazil: paragenesis and stable isotope constraints. Miner Deposita 43:129–159

Moreto CPN, Monteiro LVS, Xavier RP, Amaral WS, Santos TJS, Juliani C, Souza Filho CR (2011) Mesoarchean (3.0 and 2.86 Ga) host rocks of the iron oxide–Cu–Au Bacaba deposit, Carajás Mineral Province: U–Pb geochronology and metallogenetic implications. Miner Deposita 46:789–811

Moreto CPN, Monteiro LVS, Creaser RA, DuFrane A, Xavier RP, Amaral WS, Silva MAD, Melo HC (2013) Metallogenetic evolution of the Archean and Paleoproterozoic iron oxide Cu–Au systems in the Southern Copper Belt, Carajás Province. In: 12th SGA Biennial Meeting, 2013, Uppsala. Proceedings of the 12th SGA Biennial Meeting

Neves MP, Villas RN, Toro MAG (2006) Datação e avaliação da fonte dos metais do depósito do Sossego, região de Carajás: evidências isotópicas de Pb e Sm-Nd. In: Proceedings, Cong Bras Geol, 43, CD-ROM

Nogueira ACR, Truckenbrodt W, Pinheiro RVL (1995) Formação Águas Claras, Pré-Cambriano da Serra dos Carajás: redescrição e redefinição litoestratigráfica: Boletim Museu Paraense Emílio Goeldi 7:177–277

Ohmoto H, Goldhaber MB (1997) Sulfur and carbon isotopes. In: Barnes HL (ed) Geochemistry of hydrothermal ore deposits, 3rd edn. Wiley, New York, pp 517–611

Ohmoto H, Rye RO (1979) Isotopes of sulfur and carbon. In: Barnes HL (ed.). Geochemistry of hydrothermal ore deposits; John Whiley & Sons; p 509–561

Oliveira MA, Dall'Agnol R, Althoff FJ, Leite AAS (2009) Mesoarchean sanukitoid rocks of the Rio Maria Granite-Greenstone Terrane, Amazonian craton, Brazil. J South Am Earth Sci 27:146–160

Pestilho ALS, Monteiro LVS (2008) Caracterização petrográfica das zonas de alteração hidrotermal e paragêneses do minério de cobre e ouro do Alvo Castanha, Província Mineral de Carajás; In: IV Simpósio de Vulcanismo e Ambientes Associados, Foz do Iguaçu, Proceedings, Sociedade Brasileira de Geologia [CD-ROM]

Pidgeon RT, Macambira MJB, Lafon JM (2000) Th–U–Pb isotopic systems and internal structures of complex zircons from an enderbite from the Pium Complex, Carajás Province, Brazil: evidence for the ages of granulites facies metamorphism and the protolith of the enderbite. Chem Geol 166:159–171

Pinheiro RVL, Holdsworth RE (2000) Evolução tectonoestratigráfica dos sistemas transcorrentes Carajás e Cinzento, Cinturão Itacaiúnas, na borda leste do Craton Amazônico, Pará. Rev Brasil Geocienc 30: 597–606

Pollard PJ (2001) Sodic(−calcic) alteration associated with Fe-oxide–Cu–Au deposits: an origin via unmixing of magmatic-derived H_2O–CO_2–salt fluids. Miner Deposita 36:93–100

Requia K, Fontboté L (2001) The Salobo iron oxide copper-gold hydrothermal system, Carajás Mineral Province, Brazil, GSA Annual Meeting, Boston, Abstracts with programs, v.33, pA-2

Requia K, Stein H, Fontboté L, Chiaradia M (2003) Re–Os and Pb–Pb geochronology of the Archean Salobo iron oxide copper–gold deposit, Carajás Mineral Province, northern Brazil. Miner Deposita 38: 727–738

Ribeiro AA, Suita MTF, Sial AN, Fallick AE, Eli F, Goulard EA (2009) Geoquímica de isótopos estáveis (C, S e O) das rochas encaixantes e do minério de Cu (Au) do depósito Cristalino, Província Mineral de Carajás, Pará. Geochim Bras 23:159–176

Rodrigues EMS, Lafon JM, Scheller T (1992) Geocronologia Pb–Pb em rochas totais da Província Mineral de Carajás: primeiros resultados. In: Cong Bras Geol, 37, Abstracts, 2:183–184

Romero JAS, Lafon JM, Nogueira ACR, Soares JL (2013) Sr isotope geochemistry and Pb–Pb geochronology of the Neoproterozoic cap carbonates, Tangará da Serra, Brazil. Int Geol Rev 55:185–203

Rye RO, Ohmoto O (1974) Sulfur and carbon isotopes and ore genesis: A Review, Economic Geology, 69: 826–842

Santos PA, Feio GRL, Dall'Agnol R, Costi HT, Lamarão CN, Galarza MA (2013a) Petrography, magnetic susceptibility and geochemistry of the Rio Branco Granite, Carajás Province, southeast of Pará, Brazil. Braz J Geol 43:2–15

Santos RD, Galarza MAT, Oliveira DC (2013b) Geologia, geoquímica e geocronologia do Diopsídio-Norito Pium, Província Carajás. Bol. Museu Paraense Emílio Goeldi. Cienc. Nat., Belém, 8: 331–337

Sardinha AS, Dall'Agnol R, Gomes ACB, Macambira MJB, Galarza MA (2004) Geocronologia Pb–Pb e U–Pb em zircão de granitóides arqueanos da região de Canaã dos Carajás, Província Mineral de Carajás. In: Cong Bras Geologia, 42, Abstracts, CD-ROM

Sardinha AS, Barros CEM, Krymski R (2006) Geology, geochemistry, and U–Pb geochronology of the Archean (2.74 Ga) Serra do Rabo granite stocks, Carajás Metallogenetic Province, Northern Brazil. J South Am Earth Sci 20:327–339

Sheppard SMF (1986) Characterization and isotopic variations in natural waters. In: Valley JW, Taylor HP Jr, O'Neil JR (eds) Stable isotopes in high temperature geological processes. Mineral Soc Am Rev Mineral 16:165–183

Silva CMG, Villas RN (1998) The Águas Claras Cu-sulfide±Au deposit, Carajás Region, Pará, Brazil: geological setting, wall-rock alteration and mineralizing fluids. Rev Brasil Geocienc 28(3):315–326

Soares ADV, Macambira MJB, Santos MGS, Vieira EAP, Massoti FS, Souza CIJ, Padilha JL, Magni MCV (2001) Depósito Cu (Au) Cristalino, Serra dos Carajás, PA: Idade da mineralização com base em análises Pb–Pb em sulfetos (dados preliminares). In: VII Simpósio de Geologia da Amazônia, Abstract, CD-ROM

Souza SRB, Macambira MJB, Scheller J (1996) Novos dados geocronológicos para os granitos deformados do Rio Itacaiunas (Serra dos Carajás, PA): implicações Estratigráfica. In: Simpósio de Geologia da Amazônia, 5, Extended Abstracts, Belém, p 380–383

Sterner SM, Hall DL, Bodnar RJ (1988) Synthetic fluid inclusions. V. Solubility relations in the system NaCl–KCl–H_2O under vapor-saturated conditions. Geochim Cosmochim Acta 52:989–1005

Suzuoki T, Epstein S (1976) Hydrogen isotope fractionation between OH-bearing minerals and water. Geochim Cosmochim Acta 40: 1229–1240

Tallarico FHB (2003) O Cinturão Cupro-Aurífero de Carajás, Brasil. Ph.D. thesis, Universidade Estadual de Campinas, 229p

Tallarico FHB, McNaughton NJ, Groves DI, Fletcher IR, Figueredo BR, Carvalho JB, Rego JL, Nunes AR (2004) Geological and SHRIMP II U–Pb constraints on the age and origin of the Breves Cu–Au–(W–Bi–Sn) deposit, Carajás, Brazil. Miner Deposita 39:68–86

Tallarico FHB, Figueiredo BR, Groves DI, Kositcin N, Mcnaughton NJ, Fletcher IR, Rego JL (2005) Geology and SHRIMP U–Pb geochronology of the Igarapè Bahia deposit, Carajás copper–gold belt, brazil: an Archean (2.57 Ga) example of iron–oxide Cu–Au–(U–REE) mineralization. Econ Geol 100:7–28

Taylor BE (1992) Degassing of H_2O from rhyolite magma during eruption and shallow intrusion, and the isotopic composition of magmatic water in hydrothermal system. Geol Surv Jpn Rep 279:190–195

Taylor HP Jr (1974) The application of oxygen and hydrogen isotope studies to problems of hydrothermal, alteration and ore deposition, Economic Geology, 69: 843–883

Taylor HP Jr (1997) Oxygen and hydrogen isotope relationships in hydrothermal mineral deposits. In: Barnes HL (ed) Geochemistry of hydrothermal ore deposits. Wiley, New York, pp 229–302

Tazava E, Oliveira CG (2000) The Igarapé Bahia Au–Cu–(REE–U) deposit, Carajás Mineral Province, Northern Brazil. In: Porter TM (ed) Hydrothermal iron-oxide copper–gold and related deposits: a global perspective, vol 1. PGC Publishing, Adelaide, pp 203–212

Torresi I, Xavier RP, Bortholoto DFA, Monteiro LVS (2012) Hydrothermal alteration, fluid inclusions and stable isotope systematics of the Alvo 118 iron oxide–copper–gold deposit, Carajás Mineral Province (Brazil): implications for ore genesis. Miner Deposita 47:299–323

Trendall AF, Basei MAS, Laeter JR, Nelson DR (1998) SHRIMP zircon U–Pb constraints on the age of the Carajás formation, GrãoPará Group, Amazon Craton. J South Am Earth Sci 11:265–277

Villas RN, Santos MD (2001) The gold deposits of the Carajás mineral province: deposit types and metallogenesis. Miner Deposita 36: 300–331

Villas RN, Galarza MA, Almada MC, Viana AS, Ronzê P (2001) Geologia do depósito Igarapé Bahia/Alemão, Província Carajás, Pará. In: Jost H, Brod JA, Queiróz ET (eds) Caracterização de Depósitos Auríferos em Distritos Mineiros Brasileiros, DNPM-ADIMB, pp 215–240

Villas RN, Neves M, Sousa F, Lima L, Lamarão C, Xavier R, Fanton J, Morais R (2004) Rochas hospedeiras e alteração hidrotermal do depósito Sossego, Província Mineral de Carajás (PMC). In: Congresso Brasileiro de Geologia, 42, CD-ROM

Villas RN, Lima LFO, Neves MP, Lamarão CN, Fanton J, Morais R (2005) Relações entre deformação, alteração hidrotermal e mineralização no Depósito Cu–Au do Sossego, Província Mineral de Carajás. In: Simpósio Brasileiro de Metalogenia, Abstracts, CD-ROM

Villas RN, Neves MP, Rosa AGN (2006) The Fe oxide-Cu-Au Sossego deposit, Carajás Mineral Province, Brasil: dating of the mineralization and fluid characteristics. In: Dall'Agnol R, Rosa-Costa LT, Klein EL (eds.) Symposium on magmatism, crustal evolution, and metallogenesis of the Amazonian Craton. Abstracts Volume. Belém, PRONEX-UFPA-SBG, p 33

Wenner DB, Taylor HP Jr (1971) Temperatures of serpentinization of ultramafic rocks based on 18O/16O fractionation between coexisting serpentine and magnetite. Contrib Mineral Petrol 32: 165–168

Williams PJ, Barton MD, Johnson DA, Fontboté L, Haller A, Mark G, Oliver NHS, Marschik R (2005) Iron oxide copper–gold deposits: geology, space-time distribution, and possible modes of origin. Economic Geology 100TH Anniversary Volume, pp 371–405

Xavier RP, Wiedenbeck M, Trumbell RB, Dreher AM, Monteiro LVS, Rhede D, Araújo CEG, Torresi I (2008) Tourmaline B-isotopes fingerprint marine evaporites as the source of high-salinity ore fluids in iron-oxide-copper-gold deposits, Carajás Mineral Province (Brazil). Geology 36:743–746

Xavier RP, Monteiro LVS, Souza Filho CR, Torresi I, Carvalho ER, Dreher AM, Wiedenbeck M, Trumbull RB, Pestilho ALS, Moreto CPN (2010) The iron oxide copper-gold deposits of the Carajás Mineral Province, Brazil: an updated and critical review. In: Porter TM (ed) Hydrothermal iron oxide copper–gold & related deposits: a global perspective, v.3, advances in the understanding of IOCG deposits, PGC Publishing, Adelaide, in press

Xavier RP, Monteiro LVS, Moreto CPN, Pestilho ALS, Melo GHC, da Silva MAD, Aires B, Ribeiro C, Freitas e Silva FH (2012) The iron oxide copper-gold systems of the Carajás Mineral Province. In: Hedenquist J, Harris M, Camus F (eds) SEG special publication 16, geology and genesis of major copper deposits and districts of the world: a tribute to Richard H. Sillitoe, vol 1, 1st edn. Society of Economic Geologists, Inc, Littleton, pp 433–454

Zheng YF (1991) Calculation of oxygen isotope fractionation in metal oxides. Geochim Cosmochim Acta 55:299–2307

Zheng YF (1993) Calculation of oxygen isotope fractionation in hydroxyl-bearing silicates. Earth Planet Sci Lett 121:247–263